

Improving VAEs’ Robustness to Adversarial Attack

Matthew Willetts^{*,1,2}
Alexander Camuto^{*,1,2}
Tom Rainforth¹
Chris Holmes^{1,2}
Stephen Roberts^{2,3}

MWILLETTS@TURING.AC.UK
ACAMUTO@TURING.AC.UK
RAINFORTH@STATS.OX.AC.UK
CHOLMES@STATS.OX.AC.UK
SJROB@ROBOTS.OX.AC.UK

¹*Department of Statistics, University of Oxford*

²*Alan Turing Institute, London*

³*Oxford-Man Institute, University of Oxford*

Abstract

Variational autoencoders (VAEs) have recently been shown to be vulnerable to adversarial attacks, wherein they are fooled into reconstructing a chosen target image. However, how to defend against such attacks remains an open problem. We make significant advances in addressing this issue by introducing methods for producing adversarially robust VAEs. Namely, we first demonstrate that methods used to obtain disentangled latent representations produce VAEs that are more robust to these attacks. However, this robustness comes at the cost of reducing the quality of the reconstructions. We, therefore, introduce a new hierarchical VAE, the *Seatbelt-VAE*, which can produce high-fidelity autoencoders that are also adversarially robust. We confirm the capabilities of the Seatbelt-VAE on several different datasets and with current state-of-the-art VAE adversarial attacks.

1. Introduction

Variational autoencoders (VAEs) are a powerful approach to learning deep generative models and probabilistic autoencoders [1, 2]. However, previous work has shown that they are vulnerable to adversarial attacks [3–5], whereby an adversary attempts to fool the VAE to produce reconstructions similar to a chosen target by adding distortions to the original input as shown in Fig 1. This kind of attack can be harmful in applications where the encoder’s output is used downstream, as in [6–11]. Further, VAEs are often themselves used to protect classifiers from adversarial attack [12, 13]. Thus, ensuring VAEs are robust to adversarial attack is an important endeavour.

Despite these vulnerabilities, little progress has been made in the literature on how to *defend* VAEs from such attacks. The aim of this paper is to investigate and introduce possible strategies for defence. Further, we seek to defend VAEs in a manner that maintains reconstruction performance.

Our first contribution towards this aim is to show that regularising the variational objective (i.e. the ELBO) during training can lead to more robust VAEs. Specifically, we leverage ideas from the disentanglement literature [14] to improve VAEs’ robustness by learning simpler and smoother representations that are less vulnerable to attack. In particular, we show that the total correlation (TC) term used into encourage independence between the dimensions of the learned latent representations [15–17], also serves as an effective regulariser for learning robust VAEs.

Though a clear improvement over the standard VAE, a severe drawback of this approach is that the gains in robustness are coupled with drops in the reconstruction performance, due to the increased regularisation. Furthermore, we find that the achievable robustness with this approach can be limited (see Fig 1) and thus potentially insufficient for particularly sensitive tasks. To address this, we introduce a new TC-regularised *hierarchical* VAE: the *Seatbelt-VAE*. By using a richer latent space

*. Equal Contribution.

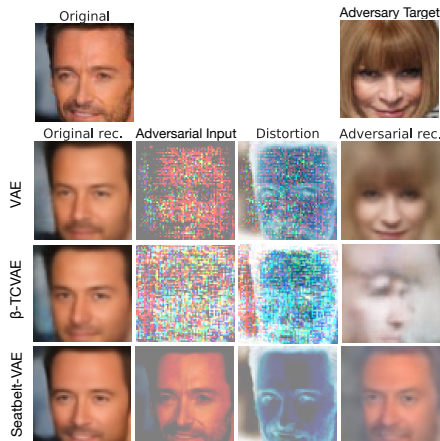


Figure 1: Adversarial attacks on CelebA for different models. Here we start with the image of Hugh Jackman and introduce an adversary that tries to produce reconstructions that look like Anna Wintour. This is done by applying a distortion (third column) to the original image to produce an adversarial input (second column). We can see that the adversarial reconstruction for the Vanilla VAE looks substantially like Wintour, indicating a successful attack. Adding a regularisation term using the β -TCVAE produces an adversarial reconstruction that does not look like Wintour, but it is also far from a successful reconstruction. Our proposed model, the Seatbelt-VAE, is sufficiently hard to attack that the output under attack still looks like Jackman, not Wintour. Note that the Seatbelt-VAE further provides a clearer reconstruction for the original image.

representation than a standard VAE, the Seatbelt-VAE can learn models which are not only even more robust to adversarial attacks than those just using TC regularisation, but can also provide reconstructions which are comparable to, and often even better than, the standard VAE.

To summarize, our key contributions are that we provide insights into what makes VAEs vulnerable to attack and how we might go about defending them. We unearth new connections between disentanglement and robustness to adversarial attack. We demonstrate that regularised VAEs, trained with an up-weighted total correlation, are significantly more robust to adversarial attacks than vanilla VAEs. Finally, we introduce a regularised hierarchical VAE, the Seatbelt-VAE, that provides further robustness to adversarial attack while providing improved reconstructions.

2. Background

2.1 Variational Autoencoders

Variational autoencoders (VAEs) are a deep extension of factor analysis suitable for high-dimensional data like images [1, 2]. They introduce a joint distribution over data \mathbf{x} and latent variables \mathbf{z} : $p_{\theta}(\mathbf{x}, \mathbf{z}) = p_{\theta}(\mathbf{x}|\mathbf{z})p(\mathbf{z})$, where $p_{\theta}(\mathbf{x}|\mathbf{z})$ is an appropriate distribution given the form of the data, the parameters of which are represented by deep nets with parameters θ , and $p(\mathbf{z}) = \mathcal{N}(0, \mathcal{I})$ is a common choice for the prior. As exact inference is intractable, one performs amortised stochastic variational inference by introducing an inference network for the latent variables, $q_{\phi}(\mathbf{z}|\mathbf{x})$, which often also takes the form of a Gaussian, $\mathcal{N}(\mathbf{z}|\mu_{\phi}(\mathbf{x}), \Sigma_{\phi}(\mathbf{x}))$. We can then perform gradient ascent, with respect to both θ and ϕ , on the evidence lower bound (ELBO)

$$\mathcal{L}(\mathbf{x}) = \mathbb{E}_{q_{\phi}(\mathbf{z}|\mathbf{x})} [\log p_{\theta}(\mathbf{x}|\mathbf{z})] - \text{KL}(q_{\phi}(\mathbf{z}|\mathbf{x})||p(\mathbf{z})), \quad (1)$$

using the reparameterisation trick to take gradients through Monte Carlo samples from $q_{\phi}(\mathbf{z}|\mathbf{x})$.

2.2 Attacking VAEs

In an adversarial attack, an agent is trying to manipulate the behaviour of some model towards a goal of their choosing, such as fooling a classifier to misclassify an image through adding a small

perturbation [18, 19]. For many deep learning models, very small changes in the input, imperceptible to the human eye, can produce large changes in the model’s output.

Attacks on VAEs have been proposed where the adversary looks to apply small input distortions that produce reconstructions close to a target adversarial image [3–5]. An example of this is shown in Fig 1, where a standard VAE is successfully attacked to turn Hugh Jackman into Anna Wintour.

The current most effective mode of attack on VAEs is known as a *latent space attack* [3–5]. This aims to find a distorted image $\mathbf{x}^* = \mathbf{x} + \mathbf{d}$ such that its posterior $q_\phi(\mathbf{z}|\mathbf{x}^*)$ is close to that of the agent’s chosen target image $q_\phi(\mathbf{z}|\mathbf{x}^t)$. This implies that the likelihood $p_\theta(\mathbf{x}^t|\mathbf{z})$ is high given draws from the posterior of the adversarial example. It is particularly important to be robust to this attack if one is concerned with using the encoder network of a VAE as part of a downstream task. For a VAE with a single stochastic layer, the latent-space adversarial objective is [3, 4]

$$\Delta(\mathbf{x}, \mathbf{d}, \mathbf{x}^t; \lambda) = \text{KL}(q_\phi(\mathbf{z}|\mathbf{x} + \mathbf{d})||q_\phi(\mathbf{z}|\mathbf{x}^t)) + \lambda\|\mathbf{d}\|_2, \quad (2)$$

where we are penalising the L_2 norm of \mathbf{d} so as to aim for attacks that change the image less. We can then simply optimise to find a good distortion \mathbf{d} .

3. Defending VAEs

Given these approaches to attacking VAEs, the critical question is now how to defend them. This problem was not considered by prior works. To address it, we first need to consider what makes VAEs vulnerable to adversarial attacks. We argue that two key factors dictate whether we can perform a successful attack on a VAE: a) whether we can induce significant changes in the encoding distribution $q_\phi(\mathbf{z}|\mathbf{x})$ through only small changes in the data \mathbf{x} , and b) whether we can induce significant changes in the reconstructed images through only small changes to the latents \mathbf{z} . The first of these relates to the *smoothness* of the encoder mapping, the latter to the smoothness of the decoder mapping.

Consider, for the sake of argument, the case where the encoder–decoder process is almost completely noiseless. Here successful reconstruction places no direct pressure for similar encodings to correspond to similar images: given sufficiently powerful networks very small changes to embeddings \mathbf{z} can imply very large changes to the reconstructed image; there is no ambiguity in the “correct” encoding of a particular datapoint. In essence, we can have lookup–table style behaviour: nearby realisations of \mathbf{z} do not necessarily relate to each other and very different images can have very similar encodings.

This will now be very vulnerable to adversarial attacks: small input changes can lead to large changes in the encoding, and small encoding changes can lead to large changes in the reconstruction. It will also tend to overfit and have gaps in the aggregate posterior, $q_\phi(\mathbf{z}) = \frac{1}{N} \sum_{n=1}^N q_\phi(\mathbf{z}|\mathbf{x}_n)$, as each $q_\phi(\mathbf{z}|\mathbf{x}_n)$ will be sharply peaked. These gaps can then be exploited by an adversary.

We postulate two possible ways to avoid this undesirable behaviour. Firstly, we can try and directly regulate the networks used by the encoder and decoder to limit the capacity of the system to have small differences in images induce large differences in latents. Secondly, we can try to regulate the level of noise in the encoding to indirectly force a smoothness in the embedding. Having a noisy encoding creates uncertainty in the latent that gives rise to a particular image, forcing similar latents to correspond to similar images. In other words, we can avoid the aforementioned vulnerabilities by either ensuring our encode–decode process is sufficiently simple, or sufficiently noisy. The fact that the VAE is vulnerable to adversarial attack suggests that its standard setup does not sufficiently encourage either of these to provide an adequate defence. Introducing additional regularisation to enforce simplicity or noisiness thus provides an intriguing prospect for defending VAEs.

Though, in principle, direct regularisation of the networks (e.g. weight decay) might be a viable defence in some scenarios, we will instead focus on indirect regularisation approaches as discussed in

the next section. The reason for this is that controlling the macroscopic behaviour of the networks through low-level regularisations can be difficult to control and, in particular, difficult to calibrate.

3.1 Disentanglement and Robustness

Recent research into disentangling VAEs [14–17, 20, 21] and the information bottleneck [22, 23] has looked to regularise the ELBO with the hope of providing more interpretable or simpler embeddings. This hints at an interesting link to robustness and raises the question: *can we use methods for encouraging disentanglement to also encourage robustness?*

Of particular relevance, [14] introduce the notion of *overlap* in the embedding of a VAE and show how controlling it is critical to achieving smooth and meaningful latent representations. Overlap encapsulates both the level of uncertainty in the encoding process and also a locality of this uncertainty: to learn a smooth representation we not only need our encoder distribution to have an appropriate entropy, we also want the different possible encodings to be similar to each other, rather than spread out. They further show that the success of many methods for disentanglement, and in particular the β -VAE [20, 22], are rooted in controlling overlap. As controlling overlap is exactly what we need to carry out for our second suggested approach to defending VAEs, we propose to train more robust VAEs by using the same ELBO regularisers as employed by disentanglement methods.

A further link between disentanglement and robustness is that disentangled representations may often also be both *simpler* and more *human-interpretable*. For example, if we were hypothetically able to learn an embedding for CelebA where one of the latent variables has a clear and smooth correspondence with hair colour, then it is likely to be difficult to conduct an adversarial attack to produce an image with a different hair colour without making substantial changes to this latent. Thus, not only might disentangled representations be more robust if they induce simpler and smoother mappings through regularisation, if they encourage human-interpretable features, this should also make it more difficult to conduct successful attacks from the perspective of human-perceived changes to the reconstruction. For instance, the definition of a successful attack is rooted in what features of an image are perceived as important to a human observer: successful attacks are those which change the qualitative nature of the reconstruction, not those which induce the largest change in individual pixels. As such, there are strong links between disentanglement and robustness through common ideas of what it means to manipulate a datapoint such as an image.

3.2 Regularising for Robustness

There are a number of different disentanglement methods that one might consider using to train robust VAEs. Perhaps the simplest would be to use a β -VAE [20], wherein we up-weight the KL term in the VAE’s ELBO by a factor $\beta \geq 1$. Indeed this is the approach that has been shown to most directly relate to overlap, with the value of β transpiring to be directly linked to the entropy of the encoder [14]. However, the β -VAE only provides disentanglement at the expense of substantial reductions in reconstruction quality as the data likelihood term has, in effect, been down-weighted [14–16]. Furthermore, the level of disentanglement it can achieve is lesser than more recent methods [15, 16].

Because of these shortfalls, we instead propose to regularise through penalisation of a total-correlation (TC) term [15, 16]. This looks to directly force independence across the different latent dimensions in aggregate posterior $q_\phi(\mathbf{z})$, such that the distribution of the data in the latent space (i.e. where we draw a datapoint at random and then pass it through the encoder) factorises across dimensions. As we are up-weighting the total correlation by β this is referred to as the β -TCVAE [16]. This

approach has been shown to provide improved disentanglement to the β -VAE, while also having a smaller deleterious effect on reconstruction quality.

To be more precise, the TC-decomposition of the VAE objective presented in [15–17, 24, 25] reveals an explicit a TC term of the variational posterior q_ϕ . The Factor and β -TCVAEs upweight this term, to produce the variational objective (with $\beta \geq 1$):

$$\mathcal{L}_{\theta, \phi; \beta, \mathbf{x}}^{\beta\text{-TC}} := \mathbb{E}_{q_\phi(\mathbf{z}|\mathbf{x})} \left[\log \frac{p_\theta(\mathbf{x}, \mathbf{z})}{q_\phi(\mathbf{z}|\mathbf{x})} \right] - (\beta - 1) \text{KL} \left(q(\mathbf{z}) \parallel \prod_j q(z_j) \right), \quad (3)$$

where j indexes over dimensions, and the TC is the term with prefactor $(\beta - 1)$. A differentiable, stochastic approximation to $\mathbb{E}_{q_\phi(\mathbf{z})}[\log q_\phi(\mathbf{z})]$ has been proposed [16, 17], rendering this decomposition possible to use as a training objective using stochastic gradient descent. However this is a biased estimator: it is a nested expectation, for which unbiased, finite-variance, estimators do not generally exist [26]. Consequently, it has the unfortunate consequence of needing large batch sizes to have the desired behaviour; for small batch sizes its practical behaviour mimics that of the β -VAE [14].

3.3 Adversarial Attacks on TC-Penalised VAEs

We now consider attacking these TC-penalised VAEs and demonstrate one of the key contributions of the paper: that empirically this form of regularisation makes adversarial attacks on VAEs via their latent space harder to carry out. To do this, we first train them under the β -TCVAE objective (i.e. Eq (12)), jointly optimising θ, ϕ for a given β . Once trained, we then attack the models using the methods outlined in Section 2.2. Namely, we use an adversary that tries to find a distortion \mathbf{d} to the input which minimises the attack loss Δ as per Eq (2).

One possible metric for how successfully such attacks have been is the achieved value reached of the attack loss Δ . If the latent space distributions for the original input and for the distorted input match exactly, then $\Delta = 0$ and the model has been completely fooled: reconstructions from samples from the attacked posterior would be indistinguishable from those from the target posterior. Meanwhile, the larger the converged value of the attack loss the less similar these distributions are and thus the more different the reconstructed image is to the adversarial target image.

We carry our these attacks for dSprites [27], Chairs [28] and 3D faces [29], for a range of β and λ values. We pick values of λ following standard methodology [3, 4], and use L-BFGS-B for gradient descent [30]. We also tried varying the dimensionality of the latent space of the model, $\|\mathbf{z}\|$, but found it had little effect on the effectiveness of the attack.

In Fig 2 we show the effect on the attack loss Δ from varying β , averaged over different original input-target pairs and over different values of $\|\mathbf{z}\|$. Note that the plot is logarithmic in the values of the loss. We see a clear pattern for each dataset that the loss values reached by the adversary increases as we increase β from the standard VAE (i.e. $\beta = 1$). This analysis is also borne out by visual inspection of the effectiveness of these attacks as shown in Fig 1 and a number of other example attacks for different datasets, β and $\|\mathbf{z}\|$, as shown in Appendix I. We will return to give further experimental results in Section 5.

An interesting point of note in Fig 2 is that in many cases the adversarial loss starts to decrease if β is set too large. As $\beta \rightarrow \infty$, there is no pressure in the objective to produce good reconstructions, and the encoder simply focuses on matching the prior regardless of the input.

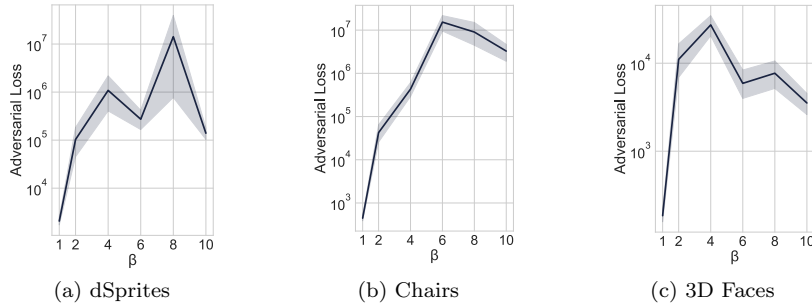


Figure 2: Attacker’s achieved loss Δ (i.e. Eq (2)) for β -TCVAE for different β values and datasets. Higher loss indicates more robustness. Shading corresponds to the 95% CI produced by attacking 10 images for each combination of $\|\mathbf{z}\| = \{4, 8, 16, 32, 64, 128\}$ and taking 50 geometrically distributed values of λ between 2^{-20} and 2^{20} (giving 3000 total trials). Note that the loss axis is logarithmic. $\beta > 1$ clearly induces a much larger loss for the adversary relative to $\beta = 1$ for all datasets.

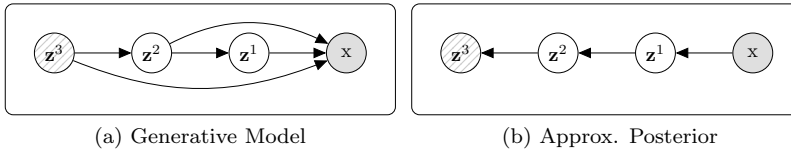


Figure 3: $L = 3$ Seatbelt-VAE. Shaded lines indicate β -TC factorisation in a given node.

4. The Seatbelt-VAE

We are now armed with the fact that penalising the TC in the ELBO induces robustness in VAEs. However, TC-penalisation in single layer VAEs comes at the expense of model reconstruction quality [16]. Our aim is to develop a model that is robust to adversarial attack while mitigating this trade-off between robustness and sample quality. To achieve this, we now consider instead using hierarchical VAEs [2, 31–33]. These are known for their superior modelling capabilities and more accurate reconstructions. As these gains stem from using more complex hierarchical latent spaces, rather than less noisy encoders, this suggests they may be able to produce better reconstructions and generative capabilities, while also remaining robust to adversarial attacks when appropriately regularised.

The simplest hierarchical extension of conditional stochastic variables in the generative model is the Deep Latent Gaussian Model (DLGM) of [2]. Here the forward model factorises as a chain:

$$p_{\theta}(\mathbf{x}, \bar{\mathbf{z}}) = p_{\theta}(\mathbf{x}|\mathbf{z}^1) \prod_{i=1}^{L-1} p_{\theta}(\mathbf{z}^i|\mathbf{z}^{i+1})p(\mathbf{z}^L), \quad (4)$$

where each $p_{\theta}(\mathbf{z}^i|\mathbf{z}^{i+1})$ is a Gaussian distribution with mean and variance parameterised by deep nets, while $p(\mathbf{z}^L)$ is an isotropic Gaussian. Unfortunately, we found that naively applying TC-correlation penalisation to DLGM-style VAEs did not confer the improved robustness we observed in single layer VAEs. We postulate that this observed weakness is inherent to the structure of chain factorisation in the generative model: this means that the data-likelihood depends solely on \mathbf{z}^1 , the bottom-most latent variable, and attackers only need to manipulate \mathbf{z}^1 to produce a successful attack.

To account for this, we instead propose a generative model in which the likelihood $p_{\theta}(\mathbf{x}|\bar{\mathbf{z}})$ depends on *all* the latent variables in the chain $\bar{\mathbf{z}}$, rather than just the bottom layer \mathbf{z}^1 . This leads to the following factorisation of the generative structure (which shares some similarity to that of BIVA [33]):

$$p_{\theta}(\mathbf{x}, \bar{\mathbf{z}}) = p_{\theta}(\mathbf{x}|\bar{\mathbf{z}}) \prod_{i=1}^{L-1} p_{\theta}(\mathbf{z}^i|\mathbf{z}^{i+1})p(\mathbf{z}^L). \quad (5)$$

To construct the ELBO, we must further introduce an inference network $q_\phi(\vec{\mathbf{z}}|\mathbf{x})$. On the basis of simplicity and that it produces effective empirical performance, we use a chain factorisation for this:

$$q_\phi(\vec{\mathbf{z}}|\mathbf{x}) = q_\phi(\mathbf{z}^1|\mathbf{x}) \prod_{i=1}^{L-1} q_\phi(\mathbf{z}^{i+1}|\mathbf{z}^i), \quad (6)$$

where each conditional distribution $q_\phi(\mathbf{z}^{i+1}|\mathbf{z}^i)$ takes the form of a Gaussian. Note that, marginalising out intermediate \mathbf{z}^i layers, we see $q_\phi(\mathbf{z}^L|\mathbf{x}) = \int \prod_{i=1}^{L-1} d\mathbf{z}^i q_\phi(\vec{\mathbf{z}}|\mathbf{x})$ is a non-Gaussian, highly flexible, distribution. A summary of the dependency structure for the generative and inference networks is shown in Fig 3 for the case $L = 3$.

To defend this model against adversarial attack, we further introduce a TC regularisation term as per the last section. We refer to the resulting model as the *Seatbelt-VAE* due to the protection it confers to adversarial attack. Because we find that, empirically, models of this type struggle to converge when TC-penalisation is applied to either the bottom-most layer or every layer, the Seatbelt-VAE only applies a TC-penalisation to the topmost latent variable \mathbf{z}^L . In other words, following the Factor and β -TCVAEs, we up-weight the term for \mathbf{z}^L of the same form as \textcircled{A} in Eq (12) to give

$$\mathcal{L}_{\theta, \phi; \beta, \mathbf{x}}^{\text{Seatbelt}} := \mathbb{E}_{q_\phi(\vec{\mathbf{z}}|\mathbf{x})} \left[\log \frac{p_\theta(\mathbf{x}, \vec{\mathbf{z}})}{q_\phi(\vec{\mathbf{z}}|\mathbf{x})} \right] - (\beta - 1) \text{KL} \left(q(\mathbf{z}^L) \parallel \prod_j q(z_j^L) \right) \quad (7)$$

where j indexes over the coordinates in \mathbf{z}^L .

Similar to analysis in single layer VAEs [15, 16], we can, in fact, reach Eq (7) by exposing this total-correlation term through an explicit decomposition of the KL (see Appendix C for a derivation). We see that, when $L = 1$, the Seatbelt-VAE reduces to a β -TCVAE. We use the $\beta = 1$ case as a baseline in our experiments as it corresponds to a Vanilla VAE for $L=1$ and for $L > 1, \beta = 1$ it produces a hierarchical model with an augmented likelihood function.

As with the β -TCVAE, training $\mathcal{L}_{\theta, \phi; \beta, D}^{\text{Seatbelt}}$ using stochastic gradient ascent with minibatches of the data is complicated by the presence of aggregate posteriors $q_\phi(\mathbf{z})$ which depend on the entire dataset. To deal with this, we derive a minibatch estimator that is a generalisation to disentangled hierarchical VAEs of the Minibatch-Weighted-Sampling estimator proposed in the context of β -TCVAEs [16, 17]. As discussed in Section 3.2, this estimator is inherently biased for finite dataset sizes, such that large batch sizes are required to provide a good estimate of the TC. See Appendix D for further details.

4.1 Attacking Seatbelt-VAE

In the Seatbelt-VAE the likelihood over data is conditioned on all layers, so manipulations to any layer have the potential to be significant. We focus on simultaneously attacking all layers, noting that, as shown in the Appendix, this is more effective than just targeting the top or base layers individually. Hence our adversarial objective for the Seatbelt-VAE is based on the following generalisation of that introduced in [3, 4] to attack all the layers at the same time:

$$\Delta^{\text{SB}}(\mathbf{x}, \mathbf{d}, \mathbf{x}^t; \lambda) = \lambda \|\mathbf{d}\|_2 + \sum_{i=1}^L \text{KL}(q_\phi(\mathbf{z}^i|\mathbf{x} + \mathbf{d}) \parallel q_\phi(\mathbf{z}^i|\mathbf{x}^t)). \quad (8)$$

We evaluate the effectiveness attack in two ways. First, we simply measure the adversary’s loss under the attack objective above. Secondly, we measure the negative adversarial likelihood of a target image \mathbf{x}^t given an attacked latent representation \mathbf{z}^* . Larger, more positive values of $-\log p_\theta(\mathbf{x}^t|\mathbf{z}^*)$ correspond to less successful attacks as they correspond to large distances between the target and the adversarial reconstruction. Highly negative values of this correspond to successful attacks as they correspond to a small distance between the adversarial target and the reconstruction.

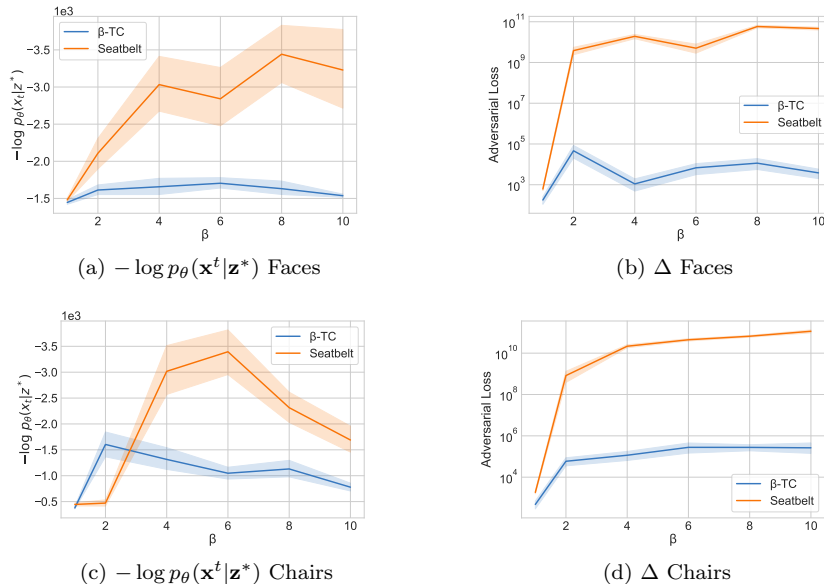


Figure 4: Numerically measuring the robustness of Seatbelt-VAEs ($L=4$) and β -TCVAEs models for different values of β . Note that the β -TCVAE with $\beta = 1$ corresponds to a vanilla VAE and that $L > 1$ $\beta = 1$ models correspond to hierarchical baselines. We show the negative adversarial likelihood of a target image \mathbf{x}^t given an attacked latent representation \mathbf{z}^* for Chairs (a) and 3D Faces (b) respectively. Larger values of $-\log p_{\theta}(\mathbf{x}^t|\mathbf{z}^*)$ correspond to less successful adversarial attacks. We also show the adversarial loss Δ in subfigures (b) and (d), which have a logarithmic axis. Shading in results corresponds to the 95% CI over variation for 10 images for each combination of $\|\mathbf{z}\| = \{4, 8, 16, 32, 64, 128\}$ and λ taking 50 geometrically distributed values between 2^{-20} and 2^{20} . As we go to the largest values of β for both Chairs and 3D Faces, Δ grows by a factor of $\approx 10^7$ and $-\log p_{\theta}(\mathbf{x}^t|\mathbf{z}^*)$ doubles for Seatbelt-VAE. β -TCVAEs do not experience such a large uptick in adversarial loss and negative adversarial likelihood. These results tell us that the Seatbelt-VAE can offer very strong protection from the adversarial attacks studied. See Appendix H.4 for heatmaps detailing these metrics for a range of Seatbelt depths (i.e varying L).

5. Experiments

We now demonstrate that Seatbelt-VAEs confer superior robustness to β -TCVAEs and standard VAEs, while preserving the ability to reconstruct inputs effectively. Through this, we demonstrate that Seatbelt-VAEs are a powerful tool for learning robust deep generative models.

We first expand on experiments in Section 3.3 and perform a battery of adversarial attacks on each of the introduced models. We randomly sample 10 input-target pairs for each dataset. Following previous work [3, 4], for each image pair we consider 50 different values of λ geometrically-distributed from 2^{-20} to 2^{20} . Thus each model undergoes 500 attacks for each attack mode. As before, we used L-BFGS-B for gradient descent [30]. We perform these experiments on Chairs [28], 3D faces [29], and CelebA [34]. Additional results for dSprites [20] can be found in Appendices H, I, and J. Details of neural network architectures and training are given in Appendix E.

We evaluate the effectiveness of adversarial attacks using the attack objective Δ as before, along with $-\log p_{\theta}(\mathbf{x}^t|\mathbf{z}^*)$, the negative likelihood of the target image (\mathbf{x}^t) given the embedding generated by the adversary (\mathbf{z}^*). Like with Δ , higher values of this metric denote a less successful attack.

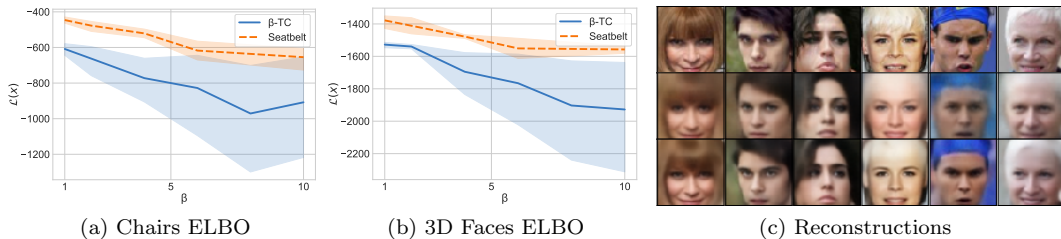


Figure 5: We show the effect of varying β on the reconstructions of TC-penalised models. In sub-figures (a) and (b) we plot the final ELBO of TC-penalised models trained on the Chairs and 3D faces, calculated *without* the β penalisation applied during training. Shading gives the 95% CI over variation due to variation of $\|\mathbf{z}\| = \{4, 8, 16, 32, 64, 128\}$ for β -TCVAE and also $L = \{2, 3, 4, 5\}$ for Seatbelt. As β increases \mathcal{L} degrades more slowly for Seatbelt-VAE, relative to β -TCVAE, (c) serves as a visual confirmation of these results. The top row shows CelebA input data. The bottom row, the reconstructions from a Seatbelt-VAE with $L = 4$ and $\beta = 20$, clearly maintains facial identity better than those from a β -TCVAE, the middle row: many of the individuals’ finer facial features lost by the β -TCVAE are maintained by the Seatbelt-VAE. Combined, these plots show the resistance of the reconstructions of Seatbelt to increasing β is visually perceptible as well as measurable. Substantial additional visual results are given in the Appendix.

5.1 Visual Appraisal of Attacks

We first visually appraise the effectiveness of attacks on vanilla VAEs, β -TCVAEs, and Seatbelt-VAEs. As mentioned in Section 1, Fig 1 shows the results of latent space attacks on three models trained on CelebA. It is apparent that the β -TCVAE provides additional resilience to the attacks compared with the standard VAE. Furthermore, this figure shows that the Seatbelt-VAE was sufficiently robust to almost completely thwart the adversary: its adversarial construction still resembles the original input. Moreover, this was achieved while also producing a clearer non-adversarial reconstructions. Additional similar examples are provided in Appendix I.

One might expect that attacks targeting a single generative factor underpinning the data would be easier for the attacker. However, we find that our models protect effectively against this as well. For example, see Appendix I.1 for plots showing an attacker attempting to rotate a dSprites heart.

5.2 Quantitative Analysis of Robustness

Having ascertained perceptually that the Seatbelt-VAE offers the strongest protection to adversarial attack, we now demonstrate this quantitatively. Fig H.10 shows $-\log p_\theta(\mathbf{x}^t | \mathbf{z}^*)$ and Δ over a range of datasets and β s for the Seatbelt-VAEs with $L = 4$ and β -TCVAEs. This figure demonstrates that the combination of depth and high TC-penalisation offers the best protection to adversarial attacks and that the Seatbelt extension confers much greater protection to adversarial attack than a single layer β -TCVAE.

In Appendix H.1, we also calculate the L_2 distance between target images and adversarial outputs and show that the loss of effectiveness of adversarial attacks is not due to the degradation of reconstruction quality from increasing β . We also include results in Appendix H for “output” attacks [4], which we find to be generally less effective. Here, the attacker directly tries to reduce the L2 distance between the reconstructed output and the target image. Again, TC-penalised models, and in particular Seatbelt-VAEs, outperformed standard VAEs.

Table 1: Robustness of downstream classification tasks under adversarial attack. We consider classifiers trained either on the reconstructed image (denoted $p(y|\tilde{\mathbf{x}})$) or on the latent representations ($p(y|\mathbf{z})$). We show accuracy when the model is attacked, resulting in perturbed embeddings \mathbf{z}^* and reconstructions ($\tilde{\mathbf{x}}^*$). Parentheses show the drop in accuracy resulting from the attack.

Dataset	Task	Accuracy by Model		
		VAE	β -TCVAE	Seatbelt-VAE
SVHN	$p(y \tilde{\mathbf{x}})$	0.12 (-0.29)	0.21 (-0.11)	0.33 (-0.09)
	$p(y \mathbf{z})$	0.13 (-0.27)	0.27 (-0.01)	0.32 (-0.07)
CIFAR10	$p(y \tilde{\mathbf{x}})$	0.16 (-0.27)	0.19 (-0.11)	0.27 (-0.14)
	$p(y \mathbf{z})$	0.12 (-0.29)	0.21 (-0.11)	0.33 (-0.09)

We also test VAE robustness to random noise where we noise the inputs and evaluate the model’s ability to reconstruct the original datapoint. Through this, we are evaluating their ability to denoise inputs. See Appendix G for an illustration of the denoising properties of TC-penalised models. This ability to denoise may partially explain these models’ robustness to attacks.

5.3 ELBO and Reconstruction Quality

Though Seatbelt-VAEs offer better protection to adversarial attack than β -TCVAEs, we also motivate their utility by way of their reconstruction quality. In Fig 5 we plot the final ELBO of the two TC-penalised models, but calculated *without* the additional β penalisation that was applied during training. We further show the effect of depth and TC-penalisation on reconstructions of CelebA. Both these plots show that Seatbelt-VAEs’ reconstructions are more resilient to increasing β than β -TCVAEs’. This resilience is both visually perceptible and measurable.

5.4 Protection to Downstream Tasks

Finally, we consider the protection that Seatbelt-VAEs might provide to downstream tasks, noting that VAEs are often used as subcomponents in larger ML systems [11], or as a mechanism to protect another model from attack [12, 13]. Table 1 shows results for classification tasks based on using 2-layer MLPs trained on either the embeddings or the reconstructions. Specifically, it shows the drop in accuracy caused by an adversary that picks a target with a different label and attacks the VAEs’ embedding using the attack objective with $\lambda = 1$. We see that Seatbelt-VAEs produced significantly better accuracies under these attacks.

6. Conclusion

We have shown that VAEs can be rendered more robust to adversarial attacks by regularising the evidence lower bound. This increase in robustness can be strengthened even further by using our proposed hierarchical VAE, the Seatbelt-VAE, which uses a carefully chosen generative structure where the likelihood makes use of all the latent variables. Designing robust VAEs is becoming pressing as they are increasingly deployed as subcomponents in larger pipelines. As we have shown, methods typically used for disentangling, motivated by their ability to provide interpretable representations, also confer robustness. Studying the beneficial effects of these methods is starting to come to the fore of VAE research [35]. We hope this work sparks further interest in the interplay between disentangling, regularisation, and model robustness.

References

- [1] Diederik P Kingma and Max Welling. Auto-encoding Variational Bayes. In *ICLR*, 2014.
- [2] Danilo Jimenez Rezende, Shakir Mohamed, and Daan Wierstra. Stochastic Backpropagation and Approximate Inference in Deep Generative Models. In *ICML*, 2014.
- [3] Pedro Tabacof, Julia Tavares, and Eduardo Valle. Adversarial Images for Variational Autoencoders. In *NIPS Workshop on Adversarial Training*, 2016.
- [4] George Gondim-Ribeiro, Pedro Tabacof, and Eduardo Valle. Adversarial Attacks on Variational Autoencoders. *CoRR*, 2018.
- [5] J Kos, I Fischer, and D Song. Adversarial Examples for Generative Models. In *IEEE Security and Privacy Workshops*, pages 36–42, 5 2018.
- [6] Weidi Xu, Haoze Sun, Chao Deng, and Ying Tan. Variational Autoencoder for Semi-supervised Text Classification. In *AAAI*, pages 3358–3364, 2017.
- [7] Matt J Kusner, Brooks Paige, and José Miguel Hernández-Lobato. Grammar Variational Autoencoder. In *ICML*, 2017.
- [8] Lucas Theis, Wenzhe Shi, Andrew Cunningham, and Ferenc Huszár. Lossy Image Compression with Compressive Autoencoders. In *ICLR*, 2017.
- [9] James Townsend, Tom Bird, and David Barber. Practical Lossless Compression with Latent Variables using Bits Back Coding. In *ICLR*, 2019.
- [10] David Ha and Jürgen Schmidhuber. World Models. In *NeurIPS*, 2018.
- [11] Irina Higgins, Arka Pal, Andrei Rusu, Loic Matthey, Christopher Burgess, Alexander Pritzel, Matthew Botvinick, Charles Blundell, and Alexander Lerchner. DARLA: Improving Zero-Shot Transfer in Reinforcement Learning. In *ICML*, 2017.
- [12] Lukas Schott, Jonas Rauber, Matthias Bethge, and Wieland Brendel. Toward the First Adversarially Robust Neural Network Model on MNIST. In *ICLR*, 2019.
- [13] Partha Ghosh, Arpan Losalka, and Michael J Black. Resisting Adversarial Attacks Using Gaussian Mixture Variational Autoencoders. In *AAAI*, 2019.
- [14] Emile Mathieu, Tom Rainforth, N. Siddharth, and Yee Whye Teh. Disentangling Disentanglement in Variational Autoencoders. In *ICML*, 2019.
- [15] Hyunjik Kim and Andriy Mnih. Disentangling by Factorising. In *NeurIPS*, 2018.
- [16] Ricky T Q Chen, Xuechen Li, Roger Grosse, and David Duvenaud. Isolating Sources of Disentanglement in Variational Autoencoders. In *NeurIPS*, 2018.
- [17] Babak Esmaeili, Hao Wu, Sarthak Jain, Alican Bozkurt, N Siddharth, Brooks Paige, Dana H Brooks, Jennifer Dy, and Jan-Willem van de Meent. Structured Disentangled Representations. In *AISTATS*, 2019.
- [18] Naveed Akhtar and Ajmal Mian. Threat of Adversarial Attacks on Deep Learning in Computer Vision: A Survey. *IEEE Access*, 6:14410–14430, 2018.
- [19] Justin Gilmer, Ryan P Adams, Ian Goodfellow, David Andersen, and George E Dahl. Motivating the Rules of the Game for Adversarial Example Research. *CoRR*, 2018.

- [20] Irina Higgins, Loic Matthey, Arka Pal, Christopher Burgess, Xavier Glorot, Matthew Botvinick, Shakir Mohamed, and Alexander Lerchner. β -VAE: Learning Basic Visual Concepts with a Constrained Variational Framework. In *ICLR*, 2017.
- [21] N Siddharth, Brooks Paige, Jan Willem Van De Meent, Alban Desmaison, Noah D Goodman, Pushmeet Kohli, Frank Wood, and Philip H.S. Torr. Learning disentangled representations with semi-supervised deep generative models. In *NeurIPS*, 2017.
- [22] Alexander A Alemi, Ian Fischer, Joshua V Dillon, and Kevin Murphy. Deep Variational Information Bottleneck. In *ICLR*, 2017.
- [23] Alexander A Alemi, Ben Poole, Ian Fischer, Joshua V Dillon, Rif A Saurous, and Kevin Murphy. Fixing a Broken ELBO. *ICML*, 2018.
- [24] Matthew D Hoffman and Matthew J Johnson. ELBO surgery: yet another way to carve up the variational evidence lower bound. In *NeurIPS*, 2016.
- [25] Alireza Makhzani, Jonathon Shlens, Navdeep Jaitly, Ian Goodfellow, and Brendan Frey. Adversarial Autoencoders. In *ICLR*, 2016.
- [26] Tom Rainforth, Robert Cornish, Hongseok Yang, Andrew Warrington, and Frank Wood. On nesting Monte Carlo estimators. In *ICML*, 2018.
- [27] Loic Matthey, Irina Higgins, Demis Hassabis, and Alexander Lerchner. dSprites: Disentanglement testing Sprites dataset, 2017.
- [28] Mathieu Aubry, Daniel Maturana, Alexei A Efros, Bryan C Russell, and Josef Sivic. Seeing 3D chairs: Exemplar part-based 2D-3D alignment using a large dataset of CAD models. In *Proceedings of the IEEE Computer Society Conference on Computer Vision and Pattern Recognition*, pages 3762–3769, 2014.
- [29] Pascal Paysan, Reinhard Knothe, Brian Amberg, Sami Romdhani, and Thomas Vetter. A 3D face model for pose and illumination invariant face recognition. In *6th IEEE International Conference on Advanced Video and Signal Based Surveillance, AVSS 2009*, pages 296–301, 2009.
- [30] Richard H Byrd, Peihuang Lu, Jorge Nocedal, and Ciyou Zhu. A Limited Memory Algorithm for Bound Constrained Optimization. *SIAM J. Sci. Comput.*, 16(5):1190–1208, 9 1995.
- [31] Casper Kaae Sønderby, Tapani Raiko, Lars Maaløe, Søren Kaae Sønderby, and Ole Winther. Ladder Variational Autoencoders. In *NeurIPS*, 2016.
- [32] Shengjia Zhao, Jiaming Song, and Stefano Ermon. Learning Hierarchical Features from Generative Models. In *ICML*, 2017.
- [33] Lars Maaløe, Marco Fraccaro, Valentin Liévin, and Ole Winther. BIVA: A Very Deep Hierarchy of Latent Variables for Generative Modeling. *NeurIPS*, 2019.
- [34] Ziwei Liu, Ping Luo, Xiaogang Wang, and Xiaoou Tang. Deep Learning Face Attributes in the Wild. In *Proceedings of International Conference on Computer Vision (ICCV)*, 2015.
- [35] Abhishek Kumar and Ben Poole. On Implicit Regularization in β -VAE. In *NeurIPS Bayesian Deep Learning Workshop*, 2019.
- [36] Matthew D Hoffman, Carlos Riquelme, and Matthew J Johnson. The β -VAE’s Implicit Prior. In *NeurIPS Bayesian Deep Learning Workshop*, 2017.

- [37] Satosi Watanabe. Information Theoretical Analysis of Multivariate Correlation. *IBM Journal of Research and Development*, 4(1):66–82, 1960.
- [38] Anthony J Bell and Terrence J Sejnowski. An information-maximisation approach to blind separation and blind deconvolution. *Neural Computation*, 7(6):1004–1034, 1995.
- [39] Yuri Burda, Roger Grosse, and Ruslan Salakhutdinov. Importance Weighted Autoencoders. In *ICLR*, 2016.
- [40] Diederik P Kingma and Jimmy Lei Ba. Adam: A Method for Stochastic Optimisation. In *ICLR*, 2015.
- [41] Tejas D Kulkarni, Will Whitney, Pushmeet Kohli, and Joshua B Tenenbaum. Deep Convolutional Inverse Graphics Network. In *NeurIPS*, 2015.
- [42] Diederik P Kingma, Tim Salimans, Rafal Jozefowicz, Xi Chen, Ilya Sutskever, and Max Welling. Improving Variational Inference with Inverse Autoregressive Flow. In *NeurIPS*, 2016.
- [43] Daniel Kunin, Jonathan M Bloom, Aleksandrina Goeva, and Cotton Seed. Loss Landscapes of Regularized Linear Autoencoders. In *ICML*, 2019.

Appendix A. Disentangling VAEs

In a β -VAE [20], a free parameter β multiplies the KL term in the evidence lower bound $\mathcal{L}(\mathbf{x})$. This objective $\mathcal{L}_\beta(\mathbf{x})$ remains a lower bound on the evidence. Later work has developed the interpretation of this model: from an information theoretic standpoint [23], and also by finding the prior on $p(\mathbf{z})$ that would give rise to this objective for $\beta < 1$ [36].

Decompositions of $\mathcal{L}(\mathbf{x})$ shed light on its meaning. As shown in [15–17, 24, 25], one can define the evidence lower bound not per data-point, but instead write it over a dataset D of size N , $D = \{\mathbf{x}^n\}$, so we have $\mathcal{L}(\theta, \phi, D)$.

[17] gives a decomposition of this dataset-level evidence lower bound:

$$\mathcal{L}(\theta, \phi, D) = -\text{KL}(q_\phi(\mathbf{z}, \mathbf{x}) \| p_\theta(\mathbf{x}, \mathbf{z})) \quad (9)$$

$$= \mathbb{E}_{q_\phi(\mathbf{z}, \mathbf{x})} \left[\underbrace{\log \frac{p_\theta(\mathbf{x}|\mathbf{z})}{p_\theta(\mathbf{x})}}_{\textcircled{1}} - \underbrace{\log \frac{q_\phi(\mathbf{z}|\mathbf{x})}{q_\phi(\mathbf{z})}}_{\textcircled{2}} \right] - \underbrace{\text{KL}(q(\mathbf{x}) \| p_\theta(\mathbf{x}))}_{\textcircled{3}} - \underbrace{\text{KL}(q_\phi(\mathbf{z}) \| p(\mathbf{z}))}_{\textcircled{4}} \quad (10)$$

where under the assumption that $p(\mathbf{z})$ factorises we can further decompose $\textcircled{4}$:

$$\text{KL}(q_\phi(\mathbf{z}) \| p(\mathbf{z})) = \mathbb{E}_{q_\phi(\mathbf{z})} \left[\underbrace{\log \frac{q_\phi(\mathbf{z})}{\prod_j q_\phi(\mathbf{z}_j)}}_{\textcircled{A}} \right] + \sum_j \underbrace{\text{KL}(q_\phi(\mathbf{z}_j) \| p(\mathbf{z}_j))}_{\textcircled{B}} \quad (11)$$

where j indexes over coordinates in \mathbf{z} . $q_\phi(\mathbf{z}, \mathbf{x}) = q_\phi(\mathbf{z}|\mathbf{x})q(\mathbf{x})$ and $q(\mathbf{x}) := \frac{1}{N} \sum_{n=1}^N \delta(\mathbf{x} - \mathbf{x}^n)$ is the empirical data distribution. $q_\phi(\mathbf{z}) := \frac{1}{N} \sum_{n=1}^N q_\phi(\mathbf{z}|\mathbf{x}^n)$ is called the *average encoding distribution* following [24].

\textcircled{A} is the total correlation (TC) for $q_\phi(\mathbf{z})$, a generalisation of mutual information to multiple variables [37]. With this mean-field $p(\mathbf{z})$, Factor and β -TCVAEs upweight this term, so we have an objective:

$$\mathcal{L}^{\beta\text{TC}}(\theta, \phi, D) = \textcircled{1} + \textcircled{2} + \textcircled{3} + \textcircled{B} + \beta \textcircled{A} \quad (12)$$

[16] gives a differentiable, stochastic approximation to $\mathbb{E}_{q_\phi(\mathbf{z})} \log q_\phi(\mathbf{z})$, rendering this decomposition simple to use as a training objective using stochastic gradient descent. We also note that \textcircled{A} , the total correlation, is also the objective in Independent Component Analysis [38].

Appendix B. Hierarchical VAEs

In a hierarchical VAE we have a set of L layers of \mathbf{z} variables: $\vec{\mathbf{z}}$. However, training DLGMs is challenging: the latent variables furthest from the data can fail to learn anything informative [31, 32]. Due to the factorisation of $q_\phi(\vec{\mathbf{z}}|\mathbf{x})$ and $p_\theta(\mathbf{x}, \vec{\mathbf{z}})$ in a DLGM, it is possible for a single-layer VAE to train in isolation within a hierarchical model: each $p_\theta(\mathbf{z}^i|\mathbf{z}^{i+1})$ distribution can become a fixed distribution not depending on \mathbf{z}^{i+1} such that each KL divergence present in the objective between corresponding \mathbf{z}^i layers can still be driven to a local minima. [32] gives a proof of this separation for the case where the model is perfectly trained, i.e. $\text{KL}(q_\phi(\mathbf{z}, \mathbf{x}) \| p_\theta(\mathbf{x}, \mathbf{z})) = 0$.

This is the hierarchical version of the collapse of \mathbf{z} units in a single-layer VAE [39], but now the collapse is over entire layers \mathbf{z}^i . It is part of the motivation for the Ladder VAE [31] and BIVA [33].

Appendix C. Derivation of ELBO for Seatbelt-VAEs

Here we derive the Seatbelt-VAE ELBO by decomposition. Specifically, now considering the ELBO for the whole dataset and using $p_{\mathcal{D}}(\mathbf{x})$ to indicate the empirical data distribution, we will obtain:

$$\begin{aligned} \mathcal{L}_{\theta, \phi; \beta, D}^{\text{Seatbelt}} &= \mathbb{E}_{q_{\phi}(\bar{\mathbf{z}}|\mathbf{x})p_{\mathcal{D}}(\mathbf{x})} [\log p_{\theta}(\mathbf{x}|\mathbf{z})] - \mathbb{E}_{q_{\phi}(\bar{\mathbf{z}}|\mathbf{x})p_{\mathcal{D}}(\mathbf{x})} \left[\sum_{i=1}^{L-1} \text{KL}(q_{\phi}(\mathbf{z}^i|\mathbf{z}^{i-1})||p_{\theta}(\mathbf{z}^i|\mathbf{z}^{i+1})) \right] \\ &\quad - \text{KL}(q_{\phi}(\mathbf{z}^L, \mathbf{z}^{L-1})||q_{\phi}(\mathbf{z}^L)q_{\phi}(\mathbf{z}^{L-1})) - \sum_j \text{KL}(q_{\phi}(\mathbf{z}_j^L)||p(\mathbf{z}_j^L)) - \beta \text{KL} \left(q_{\phi}(\mathbf{z}^L)||\prod_j q_{\phi}(\mathbf{z}_j^L) \right) \end{aligned} \quad (13)$$

where $\mathbf{z}^0 = \mathbf{x}$.

We start with the forms of p and q given in the main paper. The likelihood is conditioned on all \mathbf{z} layers: $p_{\theta}(\mathbf{x}|\bar{\mathbf{z}})$.

$$\mathcal{L}(\theta, \phi, D) = \mathbb{E}_{q_{\phi}(\bar{\mathbf{z}}, \mathbf{x})} \log \frac{p_{\theta}(\mathbf{x}, \bar{\mathbf{z}})}{\log q_{\phi}(\bar{\mathbf{z}}, \mathbf{x})} = \mathbb{E}_{q_{\phi}(\bar{\mathbf{z}}, \mathbf{x})} [\log p_{\theta}(\mathbf{x}|\bar{\mathbf{z}})] - \mathbb{E}_{q(\mathbf{x})} [\text{KL}(q_{\phi}(\bar{\mathbf{z}}, \mathbf{x})||p_{\theta}(\bar{\mathbf{z}}))] \quad (14)$$

$$= \mathbb{E}_{q(\bar{\mathbf{z}}, \mathbf{x})} \log p_{\theta}(\mathbf{x}|\bar{\mathbf{z}}) - \mathbb{E}_{q(\mathbf{x})} \log q(\mathbf{x}) + \mathbb{E}_{q(\bar{\mathbf{z}}, \mathbf{x})} \log \frac{p_{\theta}(\bar{\mathbf{z}})}{q(\bar{\mathbf{z}}|\mathbf{x})} \quad (15)$$

$$= \mathbb{E}_{q(\bar{\mathbf{z}}, \mathbf{x})} \log p_{\theta}(\mathbf{x}|\bar{\mathbf{z}}) + \mathcal{H}(q(\mathbf{x})) \quad (16)$$

$$+ \underbrace{\int d\mathbf{x} d\mathbf{z}^1 \prod_{i=2}^L (d\mathbf{z}^i q_{\phi}(\mathbf{z}^i|\mathbf{z}^{i-1})) q_{\phi}(\mathbf{z}^1|\mathbf{x}) q(\mathbf{x}) \log \frac{p(\mathbf{z}^L) \prod_{k=1}^{L-1} p_{\theta}(\mathbf{z}^k|\mathbf{z}^{k+1})}{q_{\phi}(\mathbf{z}^1|\mathbf{x}) \prod_{m=1}^{L-1} q_{\phi}(\mathbf{z}^{m+1}|\mathbf{z}^m)}}_{\textcircled{W}}$$

So here we have three terms: an expectation over the data likelihood, the entropy of the empirical data distribution (a constant) and \textcircled{W} . We now can expand \textcircled{W} to a term involving the prior for the latent \mathbf{z}^L and a term involving the conditional distributions from the generative model for the remaining components of $\bar{\mathbf{z}}$:

$$\begin{aligned} \textcircled{W} &= \underbrace{\int d\mathbf{x} \prod_{i=1}^L (d\mathbf{z}^i) q_{\phi}(\bar{\mathbf{z}}|\mathbf{x}) q(\mathbf{x}) \log \frac{p(\mathbf{z}^L)}{q_{\phi}(\mathbf{z}^L|\mathbf{z}^{L-1})}}_{\textcircled{T}} \\ &\quad + \underbrace{\int d\mathbf{x} \prod_{i=1}^L (d\mathbf{z}^i) q_{\phi}(\bar{\mathbf{z}}|\mathbf{x}) q(\mathbf{x}) \log \frac{\prod_{k=1}^{L-1} p_{\theta}(\mathbf{z}^k|\mathbf{z}^{k+1})}{q_{\phi}(\mathbf{z}^1|\mathbf{x}) \prod_{m=1}^{L-2} q_{\phi}(\mathbf{z}^{m+1}|\mathbf{z}^m)}}_{\textcircled{R}}. \end{aligned} \quad (17)$$

Now the first term, \textcircled{T} is an expectation over the KL divergence between $q_{\phi}(\mathbf{z}^L|\mathbf{z}^{L-1})$ and $p(\mathbf{z}^L)$

$$\textcircled{T} = -\mathbb{E}_{q_{\phi}(\mathbf{z}^{L-1})} \text{KL}(q_{\phi}(\mathbf{z}^L|\mathbf{z}^{L-1})||p(\mathbf{z}^L)) \quad (18)$$

This term \textcircled{T} is that which we will perform TC-decomposition on shortly. The remaining part \textcircled{R} , it that part of \textcircled{W} not involving the prior for ‘top-most’ latent variable \mathbf{z}^L , is now the subject of our attention. Now we split out the part of \textcircled{R} involving the generative and posterior terms for the

latent variable closest to the data, \mathbf{z}^1 and the rest:

$$\begin{aligned} \textcircled{\text{R}} &= \underbrace{\int d\mathbf{x} \prod_{i=1}^L (d\mathbf{z}^i) q_\phi(\bar{\mathbf{z}}|\mathbf{x}) q(\mathbf{x}) \log \frac{p_\theta(\mathbf{z}^1|\mathbf{z}^2)}{q_\phi(\mathbf{z}^1|\mathbf{x})}}_{\textcircled{\text{R}}_a} \\ &+ \underbrace{\sum_{m=2}^{L-1} \int d\mathbf{x} \prod_{i=1}^L (d\mathbf{z}^i) q_\phi(\bar{\mathbf{z}}|\mathbf{x}) q(\mathbf{x}) \log \frac{p_\theta(\mathbf{z}^m|\mathbf{z}^{m+1})}{q_\phi(\mathbf{z}^m|\mathbf{z}^{m-1})}}_{\textcircled{\text{R}}_b}. \end{aligned} \quad (19)$$

Like $\textcircled{\text{T}}$, the first of these terms $\textcircled{\text{R}}_a$ is an expectation over a KL:

$$\textcircled{\text{R}}_a = -\mathbb{E}_{q_\phi(\mathbf{z}^2, \mathbf{x})} \text{KL}(q_\phi(\mathbf{z}^1|\mathbf{x}) || p_\theta(\mathbf{z}^1|\mathbf{z}^2)). \quad (20)$$

And the rest, $\textcircled{\text{R}}_b$, provides the KL divergences in the ELBO for all latent variables other than \mathbf{z}^L and \mathbf{z}^1 . It reduces to a sum of expectations over KL divergences, one per latent variable.

$$\textcircled{\text{R}}_b = \sum_{m=2}^{L-1} \int d\mathbf{x} \prod_{i=1}^L (d\mathbf{z}^i) q_\phi(\mathbf{z}^1|\mathbf{x}) q(\mathbf{x}) \prod_{k=1, \neq m}^{L-1} (q_\phi(\mathbf{z}^{k+1}|\mathbf{z}^k)) q_\phi(\mathbf{z}^m|\mathbf{z}^{m-1}) \log \frac{p_\theta(\mathbf{z}^m|\mathbf{z}^{m+1})}{q_\phi(\mathbf{z}^m|\mathbf{z}^{m-1})} \quad (21)$$

$$= -\sum_{m=2}^{L-1} \int d\mathbf{x} \prod_{i=1}^L (d\mathbf{z}^i) q_\phi(\mathbf{z}^1|\mathbf{x}) q(\mathbf{x}) \prod_{k=1, \neq m}^{L-1} (q_\phi(\mathbf{z}^{k+1}|\mathbf{z}^k)) \text{KL}(q_\phi(\mathbf{z}^m|\mathbf{z}^{m-1}) || p_\theta(\mathbf{z}^m|\mathbf{z}^{m+1})) \quad (22)$$

$$= -\sum_{m=2}^{L-1} \mathbb{E}_{q_\phi(\mathbf{z}^{m+1}, \mathbf{z}^{m-1})} \text{KL}(q_\phi(\mathbf{z}^m|\mathbf{z}^{m-1}) || p_\theta(\mathbf{z}^m|\mathbf{z}^{m+1})). \quad (23)$$

Now we have:

$$\mathcal{L}(\theta, \phi, D) = \mathbb{E}_{q(\bar{\mathbf{z}}, \mathbf{x})} \log p_\theta(\mathbf{x}|\bar{\mathbf{z}}) + \mathcal{H}(q(\mathbf{x})) + \textcircled{\text{R}}_a + \textcircled{\text{R}}_b + \textcircled{\text{T}} \quad (24)$$

$$(25)$$

Now we wish to apply TC decomposition to the top-most latent variable \mathbf{z}^L , the KL for which is term $\textcircled{\text{T}}$. Doing this, with j indexes over units in \mathbf{z}^L .

$$\begin{aligned} \textcircled{\text{T}} &= -\mathbb{E}_{q_\phi(\mathbf{z}^{L-1})} \left[\mathbb{E}_{q_\phi(\mathbf{z}^L|\mathbf{z}^{L-1})} [\log q_\phi(\mathbf{z}^L|\mathbf{z}^{L-1}) - \log p(\mathbf{z}^L) + \log q_\phi(\mathbf{z}^L) \right. \\ &\quad \left. - \log q_\phi(\mathbf{z}^L) + \log \prod_j q_\phi(\mathbf{z}_j^L) - \log \prod_j q_\phi(\mathbf{z}_j^L)] \right] \end{aligned} \quad (26)$$

$$= -\mathbb{E}_{q_\phi(\mathbf{z}^L, \mathbf{z}^{L-1})} \left[\log \frac{q_\phi(\mathbf{z}^L|\mathbf{z}^{L-1})}{q_\phi(\mathbf{z}^L)} \right] - \mathbb{E}_{q_\phi(\mathbf{z}^L)} \left[\log \frac{q_\phi(\mathbf{z}^L)}{\prod_j q_\phi(\mathbf{z}_j^L)} \right] - \mathbb{E}_{q_\phi(\mathbf{z}^L)} \left[\log \frac{\prod_j q_\phi(\mathbf{z}_j^L)}{p(\mathbf{z}^L)} \right] \quad (27)$$

$$\begin{aligned} &= -\mathbb{E}_{q_\phi(\mathbf{z}^L, \mathbf{z}^{L-1})} \left[\log \frac{q_\phi(\mathbf{z}^L|\mathbf{z}^{L-1})q_\phi(\mathbf{z}^{L-1})}{q_\phi(\mathbf{z}^L)q_\phi(\mathbf{z}^{L-1})} \right] - \mathbb{E}_{q_\phi(\mathbf{z}^L)} \left[\log \frac{q_\phi(\mathbf{z}^L)}{\prod_j q_\phi(\mathbf{z}_j^L)} \right] \\ &\quad - \sum_j \mathbb{E}_{q_\phi(\mathbf{z}^L)} \left[\log \frac{q_\phi(\mathbf{z}_j^L)}{p(\mathbf{z}_j^L)} \right] \end{aligned} \quad (28)$$

$$\begin{aligned} &= -\underbrace{\text{KL}(q_\phi(\mathbf{z}^L, \mathbf{z}^{L-1})||q_\phi(\mathbf{z}^L)q_\phi(\mathbf{z}^{L-1}))}_{\textcircled{\text{T}}_a} - \underbrace{\text{KL}(q_\phi(\mathbf{z}^L)||\prod_j q_\phi(\mathbf{z}_j^L))}_{\textcircled{\text{T}}_b} \\ &\quad - \underbrace{\sum_j \text{KL}(q_\phi(\mathbf{z}_j^L)||p(\mathbf{z}_j^L))}_{\textcircled{\text{T}}_c} \end{aligned} \quad (29)$$

Where we have used $p(\mathbf{z}^L) = \prod_j p(\mathbf{z}_j^L)$ for our chosen generative model, a product of independent unit-variance Gaussian distributions. As in Chen et al. (2018), we choose to weight $\textcircled{\text{T}}_b$ the total correlation (for $q_\phi(\mathbf{z}^L)$) by a prefactor β .

$$\mathcal{L}^{\text{SB}}(\theta, \phi, D, \beta) = \mathbb{E}_{q(\bar{\mathbf{z}}, \mathbf{x})} \log p_\theta(\mathbf{x}|\bar{\mathbf{z}}) + \mathcal{H}(q(\mathbf{x})) + \textcircled{\text{R}}_a + \textcircled{\text{R}}_b + \textcircled{\text{T}}_a + \beta \textcircled{\text{T}}_b + \textcircled{\text{T}}_c \quad (30)$$

Giving us the ELBO for Seatbelt-VAEs, Eq (C.1).

Appendix D. Minibatch Weighted Sampling for \mathbf{z}^i

As in Chen et al. (2018), applying β -TC decomposition requires us to calculate terms of the form:

$$\mathbb{E}_{q_\phi(\mathbf{z}^i)} \log q_\phi(\mathbf{z}^i) \quad (31)$$

The $i = 1$ case is covered in the appendix of Chen et al. (2018). First we will repeat the argument for $i = 1$ as made in Chen et al. (2018), but in our notation, and then we cover the case $i > 1$ for models with factorisation of $q_\phi(\vec{\mathbf{z}}|\mathbf{x})$ of Seatbelt VAEs.

D.1 MWS for $q_\phi(\mathbf{z}^1)$: β -TCVAEs

We denote $\mathcal{B}_M = \{\mathbf{x}_1, \mathbf{x}_2, \dots, \mathbf{x}_M\}$, a minibatch of datapoints drawn uniformly iid from $q(\mathbf{x}) = 1/N \sum_{n=1}^N \delta(\mathbf{x} - \mathbf{x}_n)$. For any minibatch we have $p(\mathcal{B}_M) = \frac{1}{N^M}$. Chen et al. (2018) introduce $r(\mathcal{B}_M|\mathbf{x})$, the probability of a sampled minibatch given that one member is x and the remaining $M - 1$ points are sampled iid from $q(\mathbf{x})$, so $r(\mathcal{B}_M|\mathbf{x}) = \frac{1}{N}^{M-1}$.

$$\mathbb{E}_{q_\phi(\mathbf{z}^1)} \log q_\phi(\mathbf{z}^1) = \mathbb{E}_{q_\phi(\mathbf{z}^1, \mathbf{x})} [\log \mathbb{E}_{q(\mathbf{x})} [q_\phi(\mathbf{z}^1|\mathbf{x})]] \quad (32)$$

$$= \mathbb{E}_{q_\phi(\mathbf{z}^1, \mathbf{x})} [\log \mathbb{E}_{p(\mathcal{B}_M)} [\frac{1}{M} \sum_{m=1}^M q_\phi(\mathbf{z}^1|\mathbf{x}_m)]] \quad (33)$$

$$\geq \mathbb{E}_{q_\phi(\mathbf{z}^1, \mathbf{x})} [\log \mathbb{E}_{r(\mathcal{B}_M|\mathbf{x})} [\frac{p(\mathcal{B}_M)}{r(\mathcal{B}_M|\mathbf{x})} \frac{1}{M} \sum_{m=1}^M q_\phi(\mathbf{z}^1|\mathbf{x}_m)]] \quad (34)$$

$$= \mathbb{E}_{q_\phi(\mathbf{z}^1, \mathbf{x})} [\log \mathbb{E}_{r(\mathcal{B}_M|\mathbf{x})} [\frac{1}{NM} \sum_{m=1}^M q_\phi(\mathbf{z}^1|\mathbf{x}_m)]] \quad (35)$$

$$(36)$$

So then during training, one samples a minibatch $\{\mathbf{x}_1, \mathbf{x}_2, \dots, \mathbf{x}_M\}$ and can estimate $\mathbb{E}_{q_\phi(\mathbf{z}^1)} \log q_\phi(\mathbf{z}^1)$ as:

$$\mathbb{E}_{q_\phi(\mathbf{z}^1)} \log q_\phi(\mathbf{z}^1) \approx \frac{1}{M} \sum_{i=1}^M [\log \sum_{j=1}^M q_\phi(\mathbf{z}_i^1|\mathbf{x}_j) - \log NM] \quad (37)$$

and \mathbf{z}_i^1 is a sample from $q_\phi(\mathbf{z}^1|\mathbf{x}_i)$.

D.2 Minibatch Weighted Sampling for $q_\phi(\mathbf{z}^i), i > 1$: Seatbelt-VAEs

Here we have that $q(\vec{\mathbf{z}}, \mathbf{x}) = \prod_{l=2}^L [q_\phi(\mathbf{z}^l|\mathbf{z}^{l-1})] q_\phi(\mathbf{z}^1|\mathbf{x}) q(\mathbf{x})$. Now instead of having a minibatch of datapoints, we have a minibatch of draws of \mathbf{z}^{i-1} : $\mathcal{B}_M^{i-1} = \{\mathbf{z}_1^{i-1}, \mathbf{z}_2^{i-1}, \dots, \mathbf{z}_M^{i-1}\}$. Each member of which is the result of sequentially sampling along a chain, starting with some particular datapoint $\mathbf{x}_m \sim q(\mathbf{x})$.

For $i > 2$, members of \mathcal{B}_M^{i-1} are drawn:

$$\mathbf{z}_j^{i-1} \sim q_\phi(\mathbf{z}^{i-1}|\mathbf{z}_j^{i-2}) \quad (38)$$

and for $i = 2$:

$$\mathbf{z}_j^1 \sim q_\phi(\mathbf{z}^1|\mathbf{x}_j) \quad (39)$$

Thus each member of this batch \mathcal{B}_M^{i-1} is the descendant of a particular datapoint that was sampled in an iid minibatch \mathcal{B}_M as defined above. We similarly define $r(\mathcal{B}_M^{i-1}|\mathbf{z}^{i-1})$ as the probability of

selecting a particular minibatch \mathcal{B}_M^{i-1} of these values out from our set $\{\mathbf{z}_n^{i-1}\}$ (of cardinality N) given that we have selected into our minibatch one particular \mathbf{z}^{i-1} from these N values. Like above, $r(\mathcal{B}_M^{i-1}|\mathbf{z}^{i-1}) = \frac{1}{N}^{M-1}$

Now we can consider $\mathbb{E}_{q_\phi(\mathbf{z}^i)} \log q_\phi(\mathbf{z}^i)$ for $i > 1$:

$$\mathbb{E}_{q_\phi(\mathbf{z}^i)} \log q_\phi(\mathbf{z}^i) = \mathbb{E}_{q_\phi(\mathbf{z}^i, \mathbf{z}^{i-1})} [\log \mathbb{E}_{q_\phi(\mathcal{B}_M^{i-1})} [q_\phi(\mathbf{z}^i | \mathbf{z}^{i-1})]] \quad (40)$$

$$= \mathbb{E}_{q_\phi(\mathbf{z}^i, \mathbf{z}^{i-1})} [\log \mathbb{E}_{p(\mathcal{B}_M^{i-1})} [\frac{1}{M} \sum_{m=1}^M q_\phi(\mathbf{z}^i | \mathbf{z}_m^{i-1})]] \quad (41)$$

$$\geq \mathbb{E}_{q_\phi(\mathbf{z}^i, \mathbf{z}^{i-1})} [\log \mathbb{E}_{r(\mathcal{B}_M^{i-1} | \mathbf{z}^{i-1})} [\frac{p(\mathcal{B}_M)}{r(\mathcal{B}_M | \mathbf{x})} \frac{1}{M} \sum_{m=1}^M q_\phi(\mathbf{z}^i | \mathbf{z}_m^{i-1})]] \quad (42)$$

$$= \mathbb{E}_{q_\phi(\mathbf{z}^i, \mathbf{z}^{i-1})} [\log \mathbb{E}_{r(\mathcal{B}_M^{i-1} | \mathbf{z}^{i-1})} [\frac{1}{NM} \sum_{m=1}^M q_\phi(\mathbf{z}^i | \mathbf{z}_m^{i-1})]] \quad (43)$$

Where we have followed the same steps as in the previous subsection.

During training, one samples a minibatch $\{\mathbf{z}_1^{i-1}, \mathbf{z}_2^{i-1}, \dots, \mathbf{z}_M^{i-1}\}$, where each is constructed by sampling ancestrally. Then one can estimate $\mathbb{E}_{q_\phi(\mathbf{z}^i)} \log q_\phi(\mathbf{z}^i)$ as:

$$\mathbb{E}_{q_\phi(\mathbf{z}^i)} \log q_\phi(\mathbf{z}^i) \approx \frac{1}{M} \sum_{k=1}^M [\log \sum_{j=1}^M q_\phi(\mathbf{z}_k^i | \mathbf{z}_j^{i-1}) - \log NM] \quad (44)$$

and \mathbf{z}_k^i is a sample from $q_\phi(\mathbf{z}^i | \mathbf{z}_k^{i-1})$. In our model we only need terms of this form for $i = L$, so we have:

$$\mathbb{E}_{q_\phi(\mathbf{z}^L)} \log q_\phi(\mathbf{z}^L) \approx \frac{1}{M} \sum_{k=1}^M [\log \sum_{j=1}^M q_\phi(\mathbf{z}_k^L | \mathbf{z}_j^{L-1}) - \log NM] \quad (45)$$

and \mathbf{z}_k^L is a sample from $q_\phi(\mathbf{z}^L | \mathbf{z}_k^{L-1})$.

Appendix E. Implementation Details

All runs were done on the Azure cloud system on NC6 GPU machines.

E.1 Encoder and Decoder Architectures

We used the same convolutional network architectures as [16]. For the encoders of all our models ($q(\cdot|\mathbf{x})$) we used purely convolutional networks with 5 convolutional layers. When training on single-channel (binary/greyscale) datasets such as dSprites, 3D Faces, or Chairs the 5 layers took the following number of filters in order: $\{32, 32, 64, 64, 512\}$. For more complex RGB datasets, such as CelebA, the layers had the following number of filters in order: $\{64, 64, 128, 128, 512\}$. The mean and variance of the amortised posteriors are the output of dense layers acting on the output of the purely convolutional network, where the number of neurons in these layers is equal to the dimensionality of the latent space \mathcal{Z} .

Similarly, for the decoders ($p(\mathbf{x}|\mathbf{z})$) of all our models we also used purely convolutional networks with 6 deconvolutional layers. When training on single-channel (binary/greyscale) datasets, dSprites, 3D Faces, or Chairs, the 6 layers took the following number of filters in order: $\{512, 64, 64, 32, 32, 1\}$. For CelebA the layers had the following number of filters in order: $\{512, 128, 128, 64, 64, 3\}$. The mean of the likelihood $p(\mathbf{x}|\cdot)$ was directly encoded by the final de-convolutional layer. The variance of the decoder, σ , was fixed to 0.1.

For β -TCVAE the range of $\|\mathbf{z}\|$ values used was $\{4, 6, 8, 16, 32, 64, 128\}$. For Seatbelt-VAEs the number of units in each layer \mathbf{z}^i decreases sequentially. There is a list `z_sizes` for each dataset, and for a model of L layers that the last L entries to give $\|\mathbf{z}^i\|, i \in \{1, \dots, L\}$.

$$\{\|\mathbf{z}\|\}^{\text{dSprites}} = \{96, 48, 24, 12, 6\} \quad (46)$$

$$\{\|\mathbf{z}\|\}^{\text{Chairs}} = \{96, 48, 24, 12, 6\} \quad (47)$$

$$\{\|\mathbf{z}\|\}^{\text{3DFaces}} = \{96, 48, 24, 12, 6\} \quad (48)$$

$$\{\|\mathbf{z}\|\}^{\text{CelebA}} = \{256, 128, 64, 32\} \quad (49)$$

$$(50)$$

For Seatbelt-VAEs we also have the mappings $q_\phi(\mathbf{z}^{i+1}|\mathbf{z}^i)$ and $p_\theta(\mathbf{z}^i|\mathbf{z}^{i+1})$. These are amortised as MLPs with 2 hidden layers with batchnorm and Leaky-ReLU activation. The dimensionality of the hidden layers also decreases as a function of layer index i :

$$\|\mathbf{h}\|(q_\phi(\mathbf{z}^{i+1}|\mathbf{z}^i)) = \mathbf{h}_{\text{sizes}}[i] \quad (51)$$

$$\|\mathbf{h}\|(p_\theta(\mathbf{z}^i|\mathbf{z}^{i+1})) = \mathbf{h}_{\text{sizes}}[i] \quad (52)$$

$$\mathbf{h}_{\text{sizes}} = [1024, 512, 256, 128, 64] \quad (53)$$

To train the model we used ADAM [40] with default parameters, a cosine decaying learning rate of 0.001, and a batch size of 1024. All data was preprocessed to fall on the interval -1 to 1. CelebA and Chairs were both downsampled and cropped as in [16] and [41] respectively. We find that using *free-bits* regularisation [42] greatly ameliorates the optimisation challenges associated with DLGMs.

Appendix F. L_2 norm of encoder and decoder network weights

Table F.1: Relative change of the L_2 of Encoders and Decoders by dataset for β -TCVAE and Seatbelt-VAE ($L = 4$) when increasing β from 1 to 10. Recent work shows that for linear autoencoders, L_2 regularisation of the weights corresponds to orthogonality of the latent projections [43]. For deep models we expect that disentangling is associated with regularised decoders and more complex encoders. The decoder receives a simpler representation, but building this representation requires more calculation. As we increase β for β -TCVAEs and Seatbelt-VAEs for Chairs, 3D Faces, and CelebA the L_2 norm increases for the encoder and decreases for the decoder. A more complex encoder is more difficult to match in the latent space and regularised decoders may be contributing to the denoising properties seen in the main paper.

		Chairs	3D Faces	CelebA
		$\beta : 1 \rightarrow 10$	$\beta : 1 \rightarrow 10$	$\beta : 1 \rightarrow 10$
Encoder	β -TCVAE	+5.0%	+19.5%	+73.7%
	Seatbelt-VAE, $L = 4$	+1.0%	+2.7%	+40.2%
Decoder	β -TCVAE	-19.4%	-15.0%	-6.8%
	Seatbelt-VAE, $L = 4$	-7.6%	-6.0%	-11.4%

Appendix G. Robustness to Noise

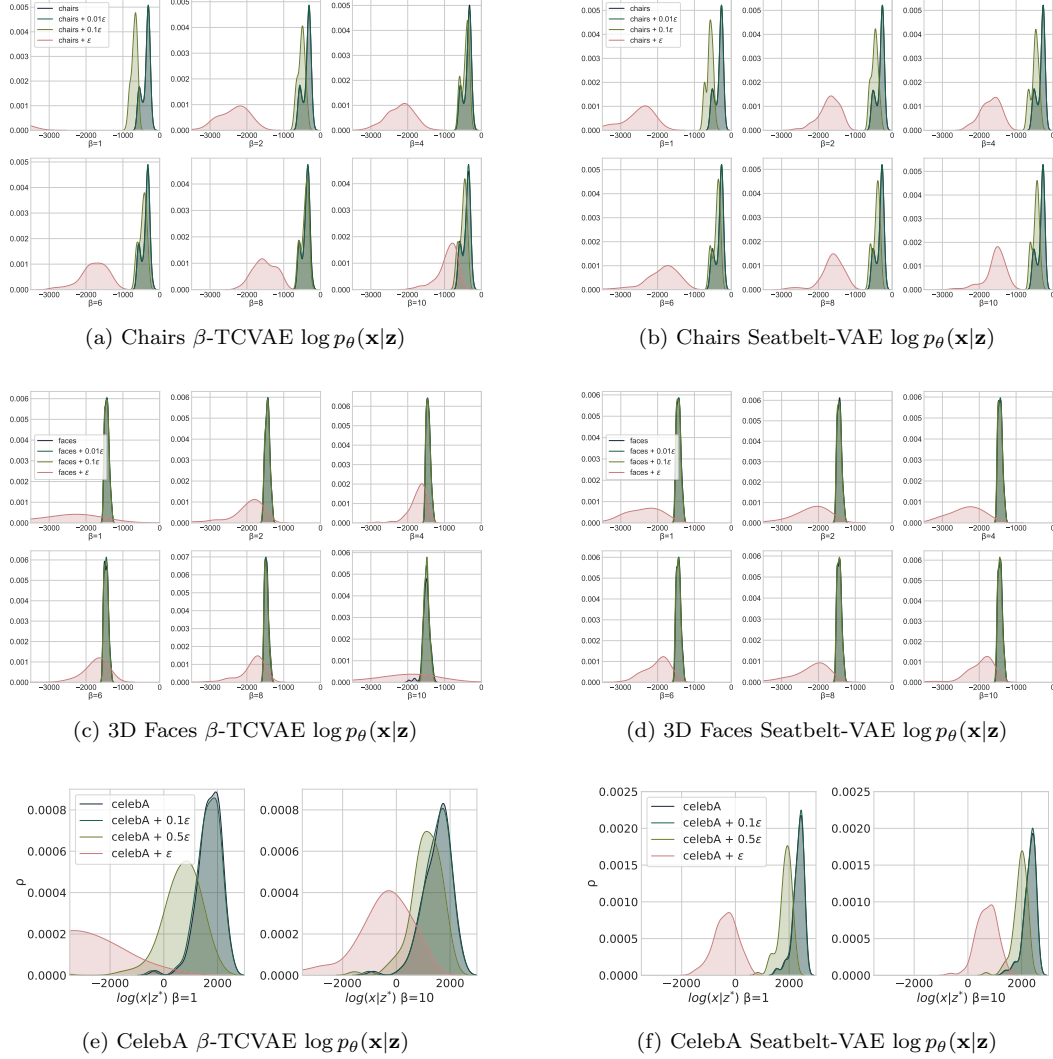


Figure G.6: Here we measure the robustness of both β -TCVAE and Seatbelt-VAE when Gaussian noise is added to Chairs, 3D Faces and CelebA; for $\mathbf{z} \sim q_{\phi}(\mathbf{z}|\mathbf{x} + a\epsilon)$ (a some scaling factor taking values in $\{0.1, 0.5, 1\}$ and $\epsilon \sim \mathcal{N}(0, 1)$) for which higher values indicate better denoising. We show these likelihood values as density plots for the β -TCVAE in (a, c, e) and for the Seatbelt-VAE with $L = 4$ in (b, d, f), taking $\beta \in \{1, 2, 4, 6, 8, 10\}$ for 3D Faces and Chairs and taking $\beta \in \{1, 10\}$ for CelebA. Note the axis scalings are different for each. We see that for both models using $\beta > 1$ produces autoencoders that are better at denoising their inputs. Namely, the mean of the density, i.e. $\mathbb{E}_{q_{\phi}(\mathbf{z}|\mathbf{x}+\epsilon)}[\log p_{\theta}(\mathbf{x}|\mathbf{z})]$, shifts dramatically to higher values for $\beta > 1$ relative to $\beta = 1$. In other words, for both these models, the likelihood of the dataset in the noisy setting is much closer to the non-noisy dataset when $\beta > 1$ across all noise scales ($0.1\epsilon, 0.5\epsilon, \epsilon$). Also note that $\log p_{\theta}(\mathbf{x}|\mathbf{z})$ is generally higher for the Seatbelt-VAE than the β -TCVAE.

Appendix H. Aggregate Analysis of Adversarial Attack

H.1 β -TCVAE

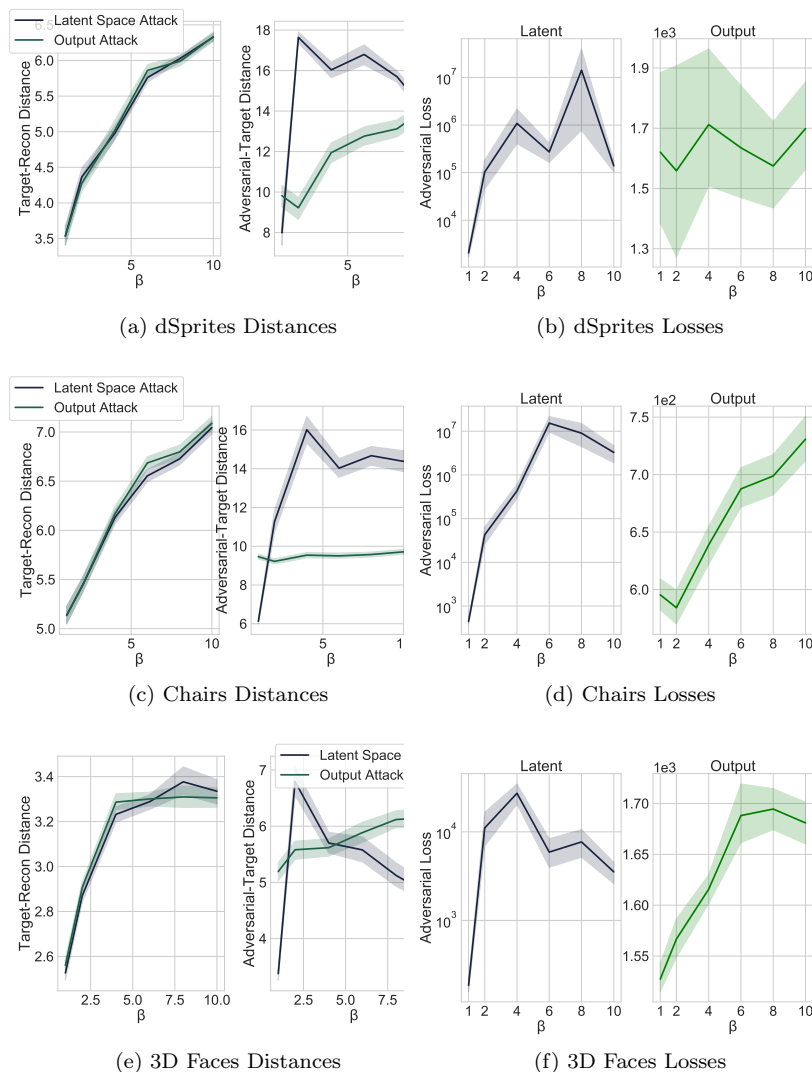


Figure H.7: Plots showing the effect of varying β in a β -TCVAE trained on dSprites (a,b), Chairs (c,d), and 3D Faces (d,e) on: the L_2 distance from the adversarial target x^t to its reconstruction when given as input (target-recon distance) and the L_2 distance between the adversarial input x^* and x^t (adversarial-target distance); and the adversarial objectives Δ . We also include these metrics for “output” attacks [4], which we find to be generally less effective. In such attacks the attacker directly tries to reduce the L2 distance between the reconstructed output and the target image. For latent attacks the adversarial-target L_2 distance grows more rapidly than the target-recon distance (i.e the degradation of reconstruction quality) as we increase β . This effect is much less clear for output attacks. This makes it apparent that the robustness we see in β -TCVAE to latent space adversarial attacks is not due the degradation in reconstruction quality we see as β increases. It is also apparent that increasing β increases the adversarial loss for latent attacks and output attacks.

H.2 Seatbelt-VAEs

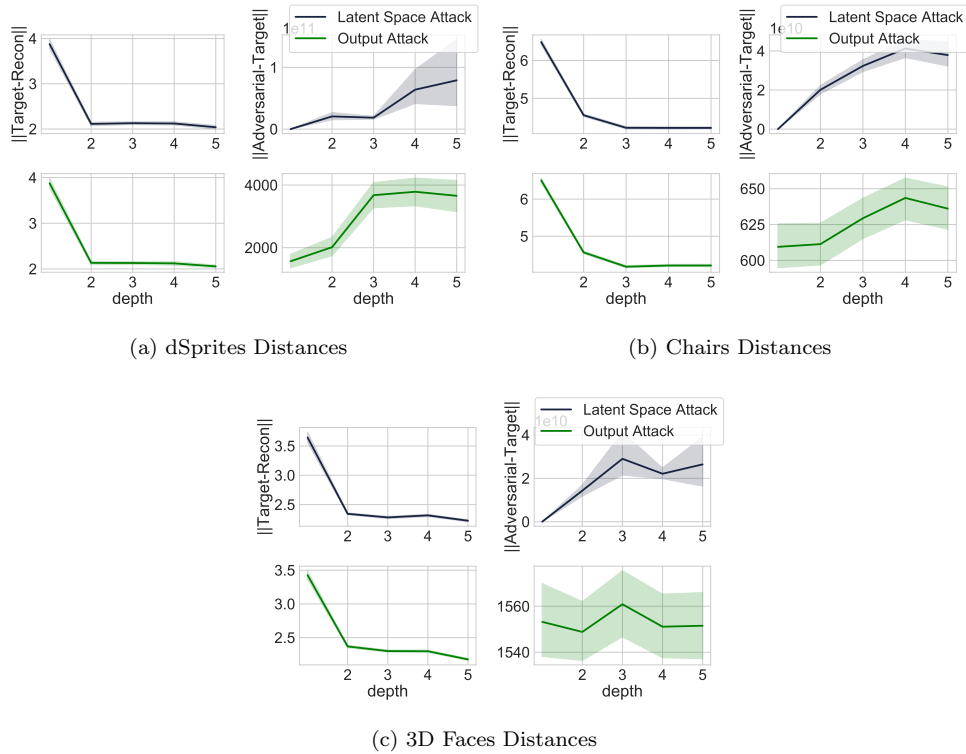
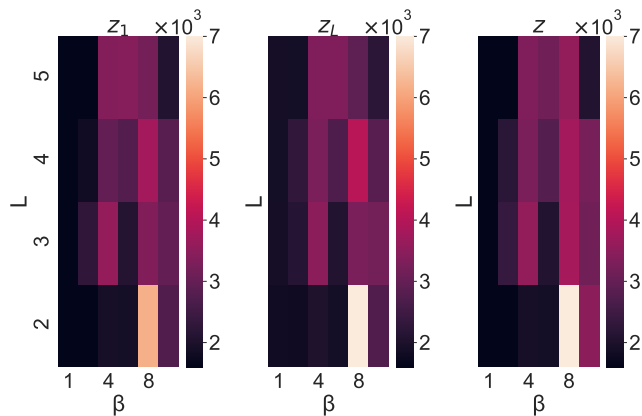
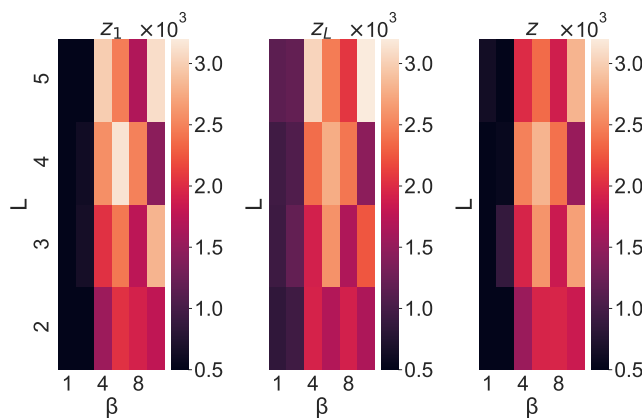


Figure H.8: Here we show the effect of increasing the number of latent variables (depth) for Seatbelt-VAEs trained on dSprites (a), 3D Faces (b) and Chairs (c) on the L_2 distance from the adversarial target x^t to its reconstruction when given as input (target-recon distance) and the L_2 distance between the adversarial input x^* and x^t (adversarial-target distance). We also include these metrics for “output” attacks [4], which we find to be generally less effective. In such attacks the attacker directly tries to reduce the L_2 distance between the reconstructed output and the target image. For both modes of attack the adversarial-target L_2 distance increases whilst the target-recon distance decreases with increasing L . This shows that the increase in depth L not only improves reconstructions but also confers part of Seatbelt models’ robustness.

H.3 Seatbelt-VAE layerwise attacks



(a) 3D Faces



(b) Chairs

Figure H.9: $-\log p_\theta(\mathbf{x}^t | \tilde{\mathbf{z}})$, $\tilde{\mathbf{z}} \sim q(\mathbf{z} | \mathbf{x} + d)$ where d is some adversarial distortion, for Seatbelt-VAEs trained on (a) 3D Faces and (b) Chairs; over β and L values for *latent* attacks. We attack the bottom layer (\mathbf{z}^1), the top layer (\mathbf{z}^L), and finally show the effect when attacking all layers (\mathbf{z}). Larger values of $-\log p_\theta(\mathbf{x}^t | \tilde{\mathbf{z}})$ correspond to less successful adversarial attacks. Generally attacking all layers seems to give the attacker a slight advantage (as seen by the slightly lower $-\log p_\theta(\mathbf{x}^t | \tilde{\mathbf{z}})$ values for Faces and Chairs).

H.4 Seatbelt-VAE attacks by model depth and β

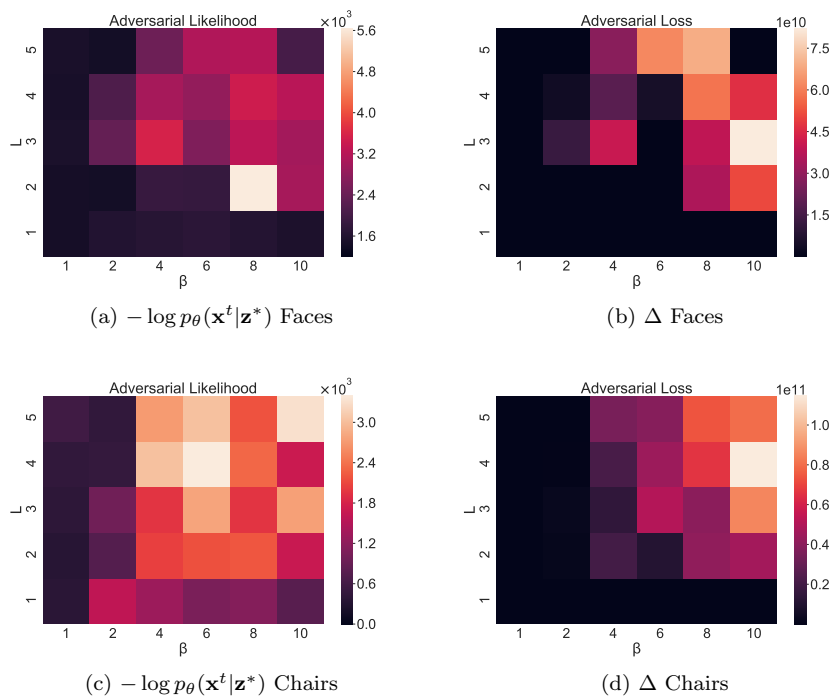


Figure H.10: Here we measure the robustness of TC-penalised models numerically. Sub-figures (a) and (c) show $-\log p_{\theta}(\mathbf{x}^t|\mathbf{z}^*)$, the adversarial likelihood of a target image \mathbf{x}^t given an attacked latent representation \mathbf{z}^* for Seatbelt-VAEs for Chairs and 3D Faces. Larger likelihood values correspond to less successful adversarial attacks. Sub-figures (b) and (d) show adversarial loss Δ for Seatbelt-VAEs for Chairs and 3D Faces. We show these likelihood and loss values over β and L (total number of stochastic layers) values for attacks. Note that the bottom rows of all figures have $L = 1$, and thus correspond to β -TCVAEs. The leftmost column corresponds to models with $\beta = 1$, which are vanilla VAEs and hierarchical VAEs. As we go to the largest values of β and L for both Chairs and 3D Faces, Δ grows by a factor of $\approx 10^7$ and $-\log p_{\theta}(\mathbf{x}^t|\mathbf{z}^*)$ doubles. These results tell us that depth and TC-penalisation together, i.e. Seatbelt-VAE, can offer immense protection from the adversarial attacks studied.

Appendix I. Adversarial Attack Plots

I.1 dSprites Adversarial Attack on a Single Factor

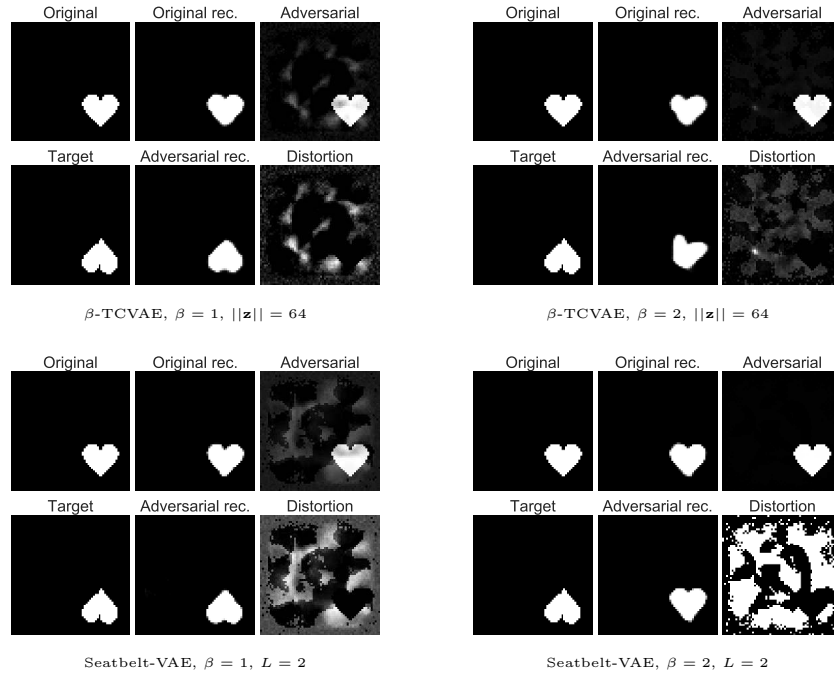


Figure I.11: Latent space attacks on rotation only of a heart-shaped dSprite for β -TCVAEs and Seatbelt-VAEs for $\beta = \{1, 2\}$. The attacks are conducted by applying a distortion (third column of each image) to the original image (top first column) to produce an adversarial input (bottom second column of each image) to try and output the target image (bottom first column). Here we show the most successful adversarial distortion in terms of adversarial loss for each model. It is apparent that the Seatbelt model is the most resilient to attack.

I.2 dSprites Adversarial Attack

I.2.1 β -TCVAEs

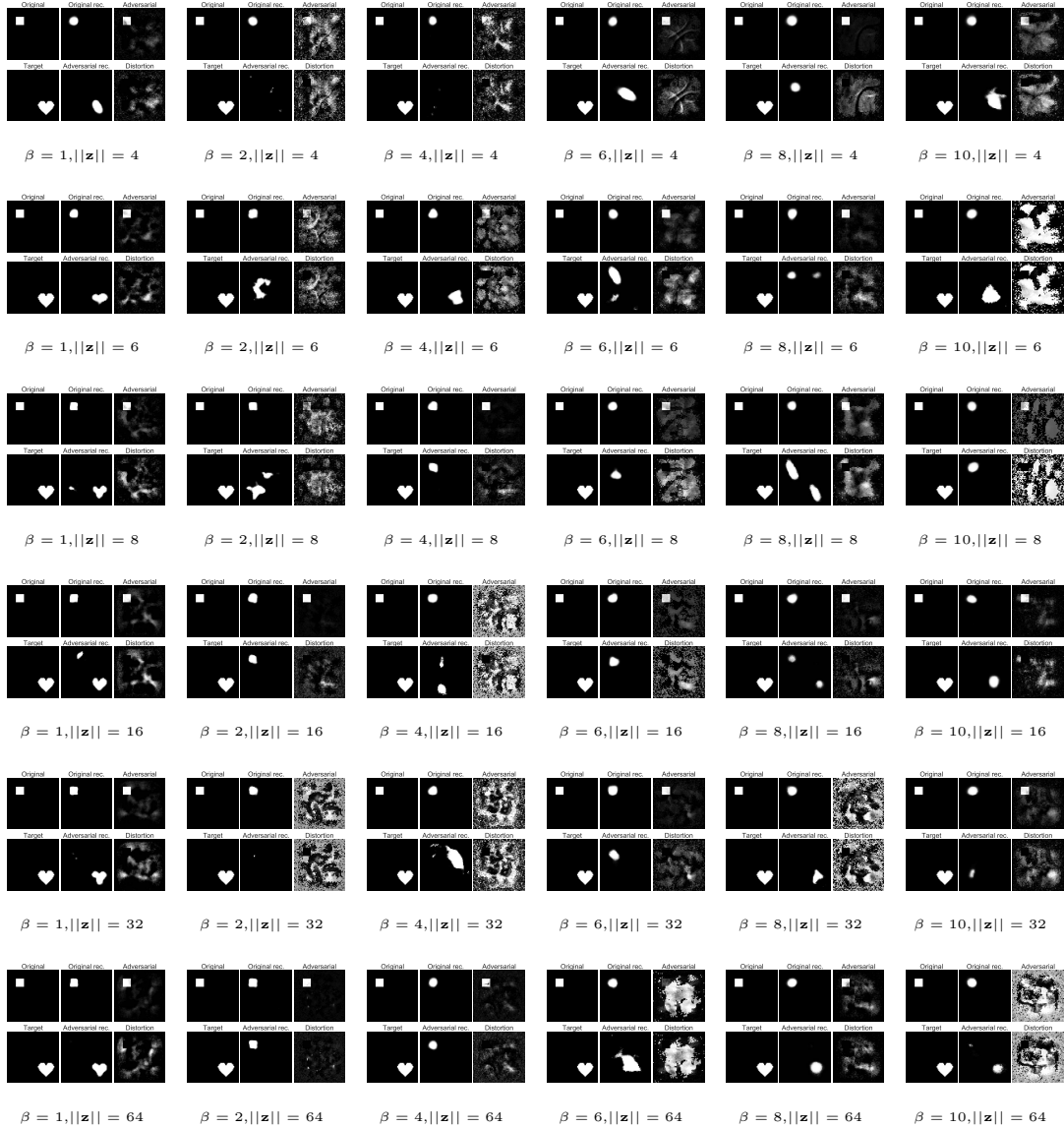


Figure I.12: Latent attacks on dSprites on β -TCVAEs for $\beta = \{1, 2, 4, 6, 8, 10\}$ and $\|z\| = \{4, 6, 8, 16, 32, 64\}$. The attacks are conducted by applying a distortion (third column of each image) to the original image (top first column) to produce an adversarial input (bottom second column of each image) to try and output the target image (bottom first column). Here we show the most successful adversarial distortion in terms of adversarial loss for each model. It is apparent that $\beta > 1$ models are the most resilient to attack.

I.2.2 SEATBELT-VAES

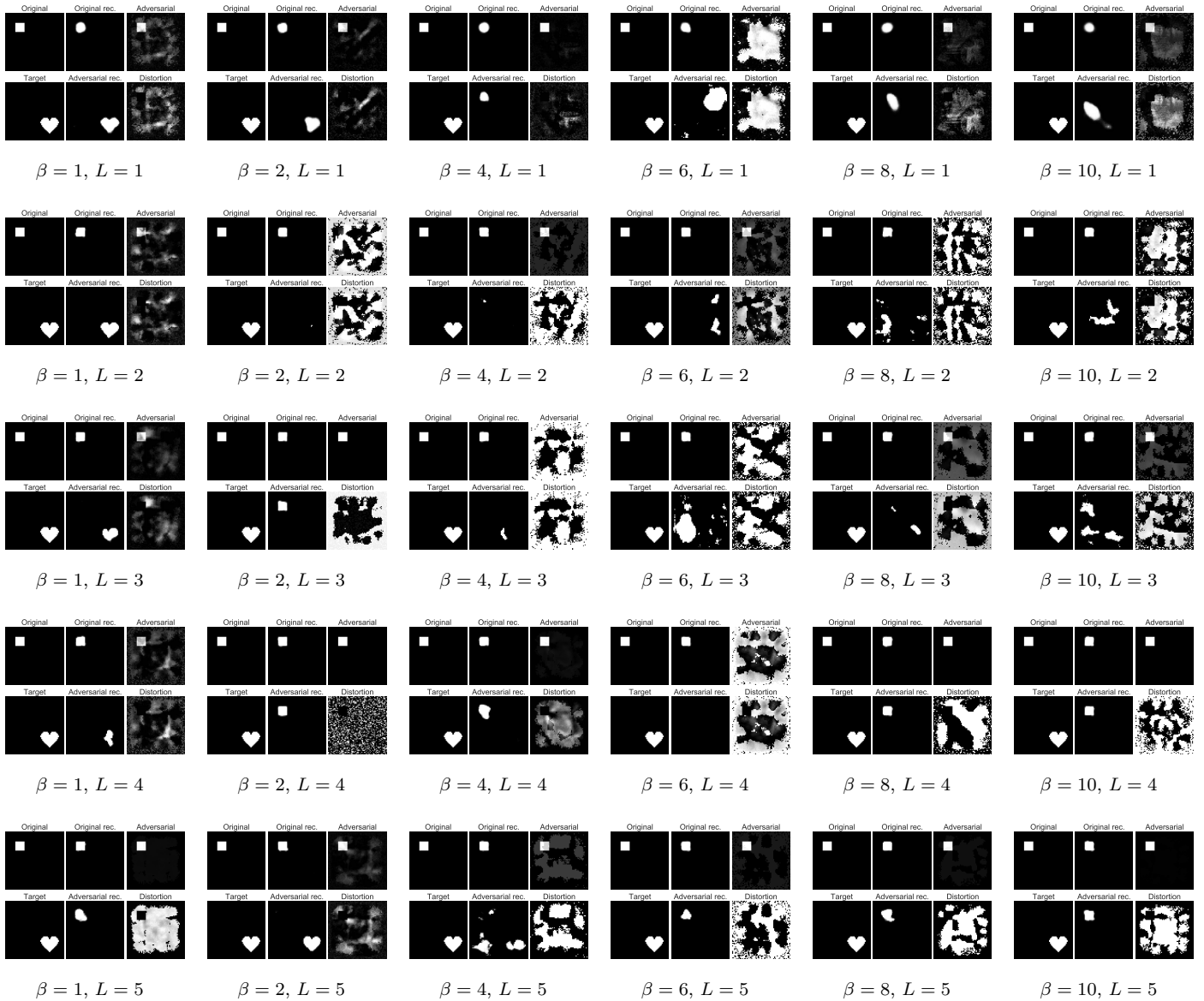


Figure I.13: Latent attacks on dSprites for Seatbelt-VAEs for $\beta = \{1, 2, 4, 6, 8, 10\}$ and $L = \{1, 2, 3, 4, 5\}$. The attacks are conducted by applying a distortion (third column of each image) to the original image (top first column) to produce an adversarial input (bottom second column of each image) to try and output the target image (bottom first column). Here we show the most successful adversarial distortion in terms of adversarial loss for each model. It is apparent that $\beta > 1$ models are the most resilient to attack.

I.3 Chairs Adversarial Attack

I.3.1 β -TCVAEs

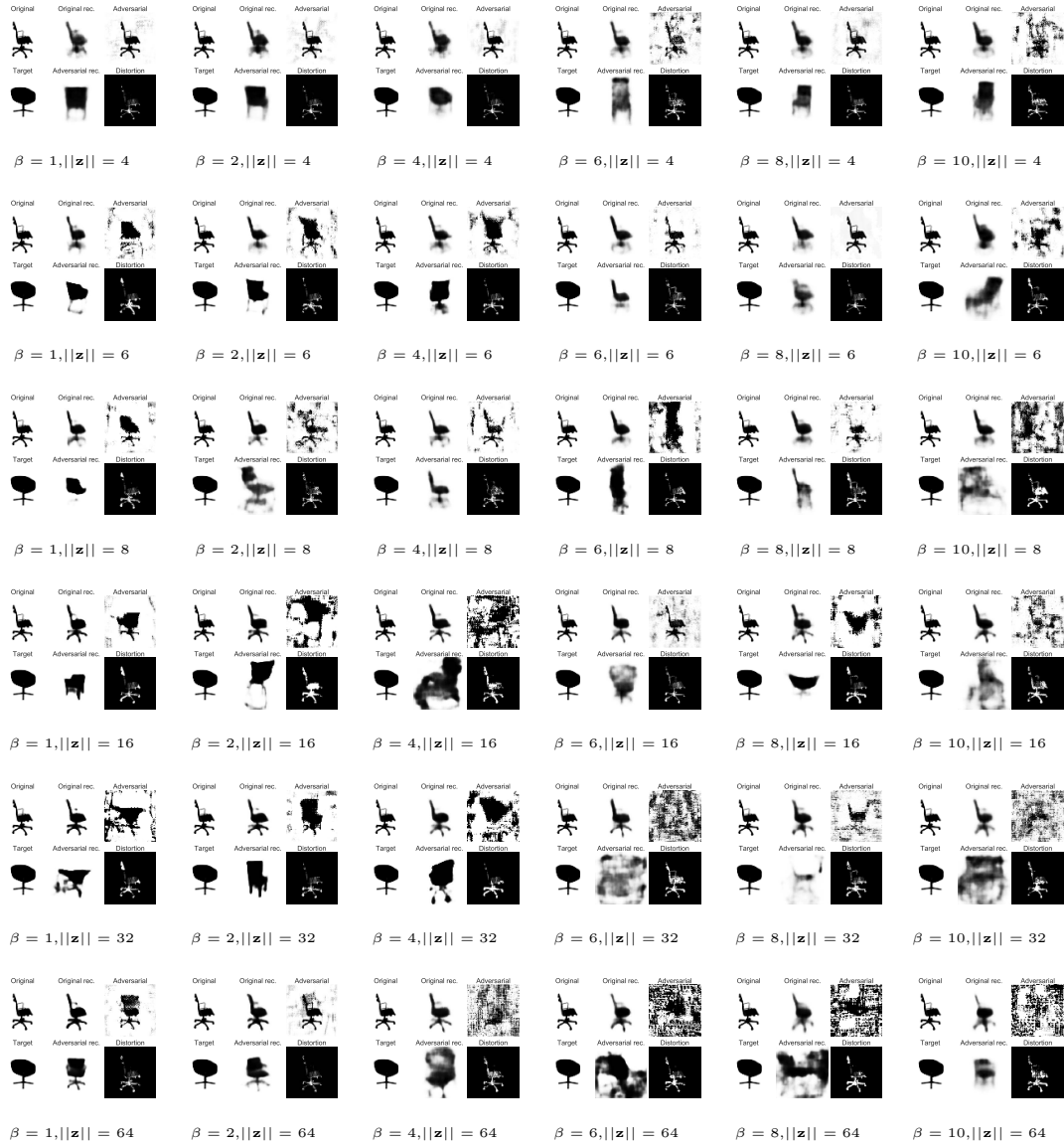


Figure I.14: Latent attacks on Chairs for β -TCVAEs for $\beta = \{1, 2, 4, 6, 8, 10\}$ and $\|\mathbf{z}\| = \{4, 6, 8, 16, 32, 64\}$. The attacks are conducted by applying a distortion (third column of each image) to the original image (top first column) to produce an adversarial input (bottom second column) to try and output the target image (bottom first column). Here we show the most successful adversarial distortion in terms of adversarial loss for each model. It is apparent that $\beta > 1$ models are the most resilient to attack.

I.3.2 SEATBELT-VAES

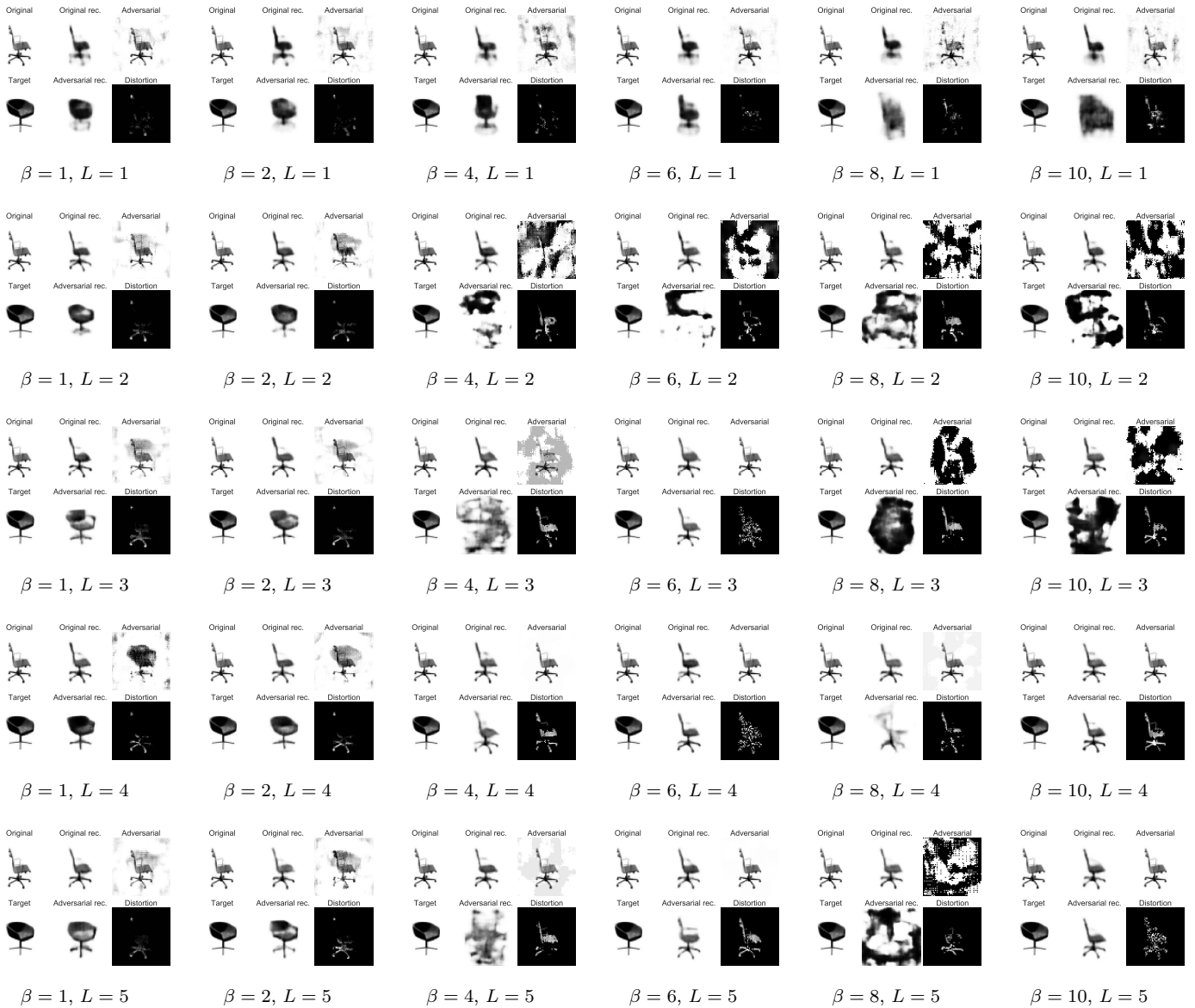


Figure I.15: Latent attacks on Chairs for Seatbelt-VAEs for $\beta = \{1, 2, 4, 6, 8, 10\}$ and $L = \{1, 2, 3, 4, 5\}$. The attacks are conducted by applying a distortion (third column of each image) to the original image (top first column) to produce an adversarial input (bottom second column of each image) to try and output the target image (bottom first column). Here we show the most successful adversarial distortion in terms of adversarial loss for each model. It is apparent that $\beta > 1$ models are the most resilient to attack with many attacks resulting in reconstructions resembling the original non-adversarial input.

I.4 3D Faces Adversarial Attack

I.4.1 β -TCVAEs



Figure I.16: Latent attacks on 3D Faces for β -TCVAEs for $\beta = \{1, 2, 4, 6, 8, 10\}$ and $\|\mathbf{z}\| = \{4, 6, 8, 16, 32, 64\}$. The attacks are conducted by applying a distortion (third column of each image) to the original image (top first column) to produce an adversarial input (bottom second column of each image) to try and output the target image (bottom first column). Here we show the most successful adversarial distortion in terms of adversarial loss for each model. It is apparent that $\beta > 1$ models are the most resilient to attack.

I.4.2 SEATBELT-VAES

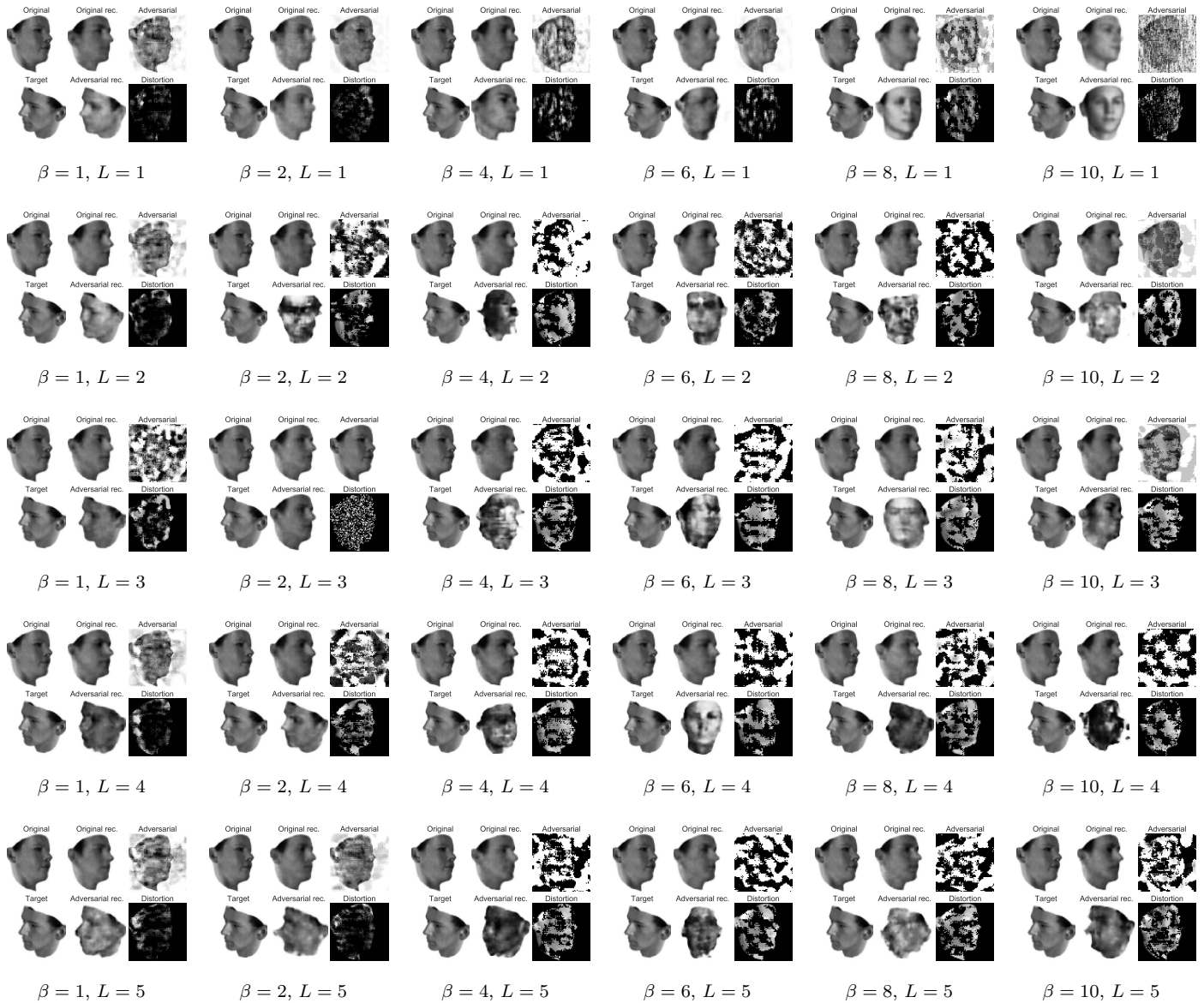


Figure I.17: Latent attacks on 3D Faces for Seatbelt-VAEs for $\beta = \{1, 2, 4, 6, 8, 10\}$ and $L = \{1, 2, 3, 4, 5\}$. The attacks are conducted by applying a distortion (third column of each image) to the original image (top first column) to produce an adversarial input (bottom second column of each image) to try and output the target image (bottom first column). Here we show the most successful adversarial distortion in terms of adversarial loss for each model. It is apparent that $\beta > 1$ models are the most resilient to attack with many attacks resulting in reconstructions resembling the original non-adversarial input.

I.5 CelebA Adversarial Attack

I.5.1 β -TCVAEs

Latent Attacks

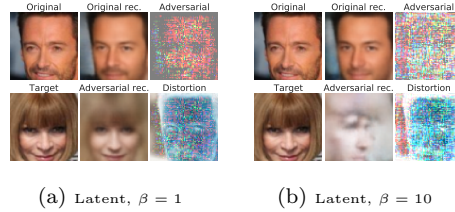


Figure I.18: Latent attacks on CelebA on β -TCVAEs for $\beta = \{1, 10\}$ and $\|\mathbf{z}\| = 32$. The attacks are conducted by applying a distortion (third column of each image) to the original image (top first column) to produce an adversarial input (bottom second column of each image) to try and output the target image (bottom first column). Here we show the most successful adversarial distortion in terms of adversarial loss for each model. It is apparent that $\beta > 1$ models are the most resilient to attack.

I.5.2 SEATBELT-VAES

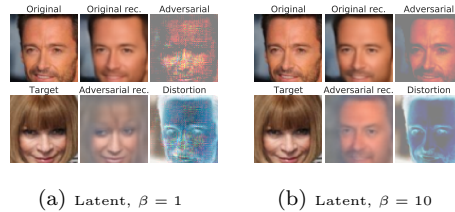


Figure I.19: Latent attacks on CelebA on $L = 4$ Seatbelt-VAEs for $\beta = \{1, 10\}$. The attacks are conducted by applying a distortion (third column of each image) to the original image (top first column) to produce an adversarial input (bottom second column of each image) to try and output the target image (bottom first column). Here we show the most successful adversarial distortion in terms of adversarial loss for each model. It is apparent that $\beta > 1$ models are the most resilient to attack with many attacks resulting in reconstructions resembling the original non-adversarial input.

Appendix J. Data Generation from Models

Ancestral Sampling in CelebA



Figure J.20: Means of the decoder from ancestral sampling in \mathbf{z} , for Seatbelt-VAEs with $L = \{1, 4\}$, $\beta = \{1, 10\}$. Note that there is a reduction in diversity of the samples for $L = 1$ (ie a β -TC VAE), $\beta = 10$, which is not the case for the samples from the $\beta = 10$ $L = 4$ Seatbelt-VAE. This illustrates perceptually that Seatbelt-VAEs are more robust to the degradation in generative model quality as β increases.

Latent Traversals for dSprites



(a) Seatbelt-VAE

Figure J.21: Latent traversals in the $|z| = 6$ top layer of $L = 2$, $\beta = 2$ for a Seatbelt-VAE trained on dSprites. Note that the traversals do not capture the ground-truth factors of variation. Disentangling in hierarchical models remains an open problem.